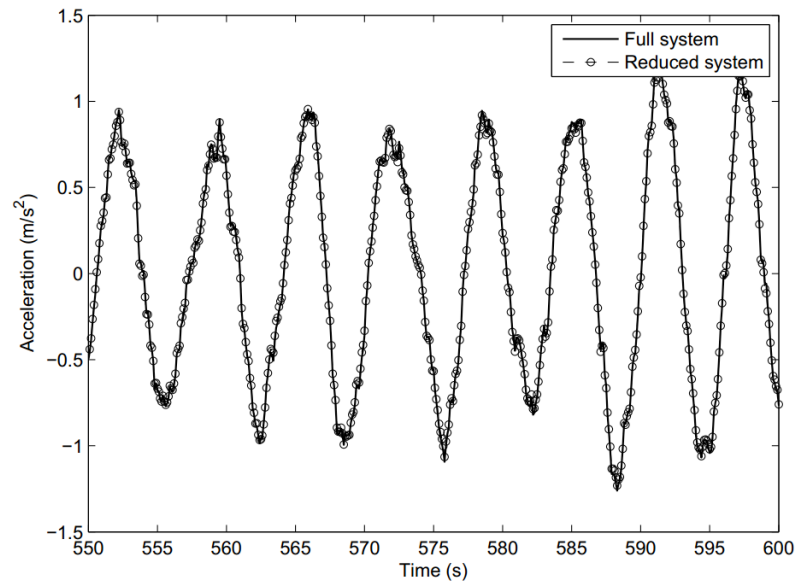




LUND
UNIVERSITY



WIND-INDUCED VIBRATIONS IN HIGH-RISE BUILDINGS

FREDRIK STEFFEN

Structural
Mechanics

Master's Dissertation

DEPARTMENT OF CONSTRUCTION SCIENCES

STRUCTURAL MECHANICS

ISRN LUTVDG/TVSM--16/5211--SE (1-66) | ISSN 0281-6679

MASTER'S DISSERTATION

WIND-INDUCED VIBRATIONS IN HIGH-RISE BUILDINGS

FREDRIK STEFFEN

Supervisor: **PETER PERSSON**, PhD, Div. of Structural Mechanics, LTH.

Examiner: Professor **PER-ERIK AUSTRELL**, Div. of Structural Mechanics, LTH.

Copyright © 2016 Division of Structural Mechanics,
Faculty of Engineering LTH, Lund University, Sweden.

Printed by Media-Tryck LU, Lund, Sweden, June 2016 (*PI*).

For information, address:

Division of Structural Mechanics,
Faculty of Engineering LTH, Lund University, Box 118, SE-221 00 Lund, Sweden.

Homepage: www.byggmek.lth.se

Abstract

Buildings are getting taller due to increased urbanisation and densification of cities. More advanced construction methods and the desire to construct impressive buildings is also supporting the trend. Due to their inherent slenderness resulting in low eigenfrequencies, these buildings are susceptible to wind-induced vibrations which can be highly disturbing for occupants. Already barely perceivable acceleration levels within the low-frequency range relevant to whole-body vibrations can cause nausea and discomfort, while high acceleration levels can cause alarm and fear amongst the occupants. The thesis summarises acceptable acceleration levels in high-rise buildings (here referred to as buildings over 200 m in height) stated in different building codes and previous work on the subject. Equations for estimating acceleration in tall buildings in an early design stage are formulated. Accelerations of a high-rise building subjected to wind-loads are evaluated using a full numerical model and one reduced with Ritz-vectors and the results are compared. The thesis focusses on wind-load dynamics in early stages of the design process, with an intent to give an indication of the dynamic properties of a building. Finally some actions to reduce vibrations are discussed.

Acknowledgements

This master thesis was carried out at the Division of Structural Mechanics, Faculty of Engineering LTH at Lund University, and concludes five years of civil engineering studies.

First and foremost, I would like to thank my supervisor Peter Persson, who has not only helped me through the work of this thesis, but also career wise. Your time and effort have been truly helpful.

I would like to thank Per-Erik Austrell for suggesting the idea of using Ritz-vectors and helping me throughout this thesis. Furthermore I would like to thank Kent Persson for always having his doors open for discussion.

Last but not least I would like to thank the other students writing their theses, both at the Division of Structural Mechanics and the Division of Structural Engineering. You know who you are, and you have made this final semester at Lund University a great one.

Lund, June 2016.

Fredrik Steffen

Contents

Abstract	i
Acknowledgements	iii
1 Introduction	3
1.1 Background	3
1.2 Scope of the thesis	4
2 Vibrations in high-rise buildings	5
2.1 Performed studies and experiments	5
2.1.1 Field experiments and surveys	5
2.1.2 Motion simulators and shaker table experiments	7
2.2 Recommendations and codes	8
2.3 Wind tunnel testing	11
3 Acceleration formulas	13
3.1 Along-wind response	13
3.2 Across-wind response	21
4 Numerical modelling and simulations	25
4.1 Ritz vectors	28
4.2 Equivalent static wind-load	29
4.3 Wind-load time series	31
4.4 Dynamic analysis and results	33
5 Vibration-reduction measures	39
5.1 Structural methods	39
5.2 Passive methods	41
5.3 Active methods	47
6 Conclusion and discussion	49
A Appendix	51

A.1	Appendix A	51
A.2	Appendix B	57
A.3	Appendix C	59

1. Introduction

1.1 Background

With advancement in material and construction sciences, buildings have been getting taller and taller during the last century. High-strength steel, lighter cladding and modern construction techniques have resulted in tall buildings, this also giving more slender buildings with lower natural frequencies. Buildings exposed to stochastic loading such as earthquake or wind load have a tendency to vibrate in the first natural frequency, i.e. the fundamental frequency. For high-rise buildings the fundamental frequency can be lower than 1 Hz. In designing these tall buildings serviceability criteria are often harder to fulfil than the survivability ones. Given the development, many international building codes have been revisited to estimate acceleration levels in tall buildings. The Eurocode on the other hand, has not been updated to accommodate the need of estimating acceleration levels in taller buildings in the preliminary design stage. It is only valid up to 200 meters and does not provide a way of estimating response in the across-wind direction due to vortex shedding. Furthermore, the Eurocode does not provide any guidelines on allowed acceleration levels at certain frequencies, nor their recurrence.

Due to their tall and slender shape, thus a low first natural frequency, tall buildings have a tendency to vibrate in their first mode. This combined with numerical models having a large number of dofs, the use of Ritz-vectors may be suitable for reducing the system in dynamic analysis. A building with many dofs has been modelled and subjected to the wind-load. The timeseries of the wind-load will be created using an inverted FFT procedure (IFFT) and applied to the finite element method (FEM) model. The time to complete the analysis will be measured and compared to the time to complete simulations in a system reduced by Ritz-vectors.

In the last chapter of the thesis, some measures of damping tall buildings are discussed.

1.2 Scope of the thesis

The thesis covers wind-loads generated by synoptic winds. Extreme wind-events such as hurricanes, tropic cyclones and downbursts are not covered. The wind load was applied in two direction, the along- and across-wind direction respectively. The FEM-model has a symmetric cross-section with centre of mass as well as moment of inertia coinciding on each floor. The system was reduced to its first mode of vibration, higher modes being neglected.

2. Vibrations in high-rise buildings

Since tall buildings with low natural frequencies vibrates due to wind excitation, it is important to have an understanding how it affects the users. This chapter aims to give a fundamental understanding on human response to low frequency accelerations and what might be considered acceptable accelerations in tall buildings.

2.1 Performed studies and experiments

Throughout the years several studies has been conducted on the human perception of vibrations in the frequency span below 1 Hz. The studies usually fall within one of three types of studies: [1]

- Field experiments and surveys of occupants in tall building.
- Motion simulator and shaker table experiments.
- Field experiments in artificially excited buildings.

The results of several studies have been summarised by Kwok et al. [1] and some of those which fall within the first two categories mentioned above is discussed below. Few, if any, field experiments in an artificially excited building with a natural frequency below 1 Hz, which is usually associated with very tall buildings, have been done and will therefore not be reviewed.

2.1.1 Field experiments and surveys

Field experiments and surveys can be divided into two categories. The first being surveys conducted in buildings during or after a passing storm. The results of the survey are later on compared to data measured from wind-tunnel testing of that particular building. More useful result have been derived from buildings that are known to have complaints from tenants regarding uncomfortable acceleration levels. This has allowed testers to properly install equipment to be able to register the actual accelerations and vibrations, and be able to compare these to what the occupants experience.

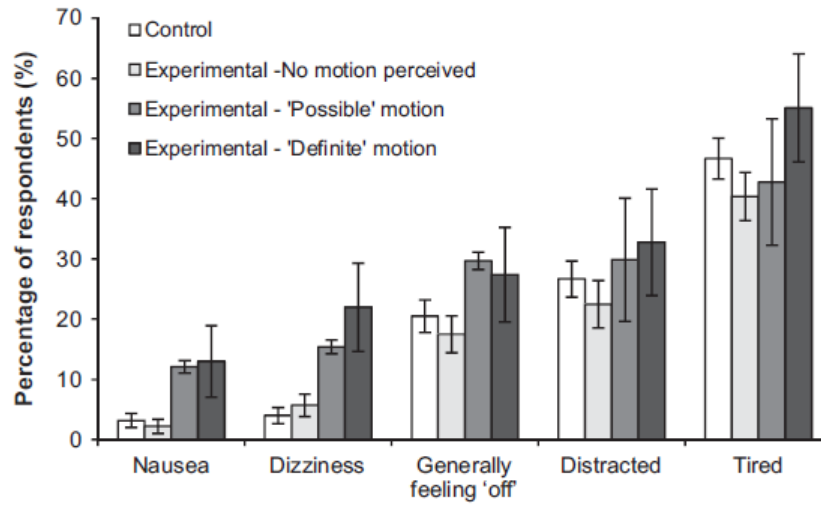


Figure 2.1: Reported symptoms of motions sickness in the study [7].

Hansen et al. [2] installed one out of two 167 m tall office buildings with accelerometers and recorded a RMS acceleration of 2 mg. Surveys showed that occupants had different cues for perceiving the motion, such as feeling, hearing, seeing etc. With owners and developers it was established that 2% of the occupants in the top third of the building could object to vibrations once a year without affecting the rental program. A limit of RMS acceleration of 5 mg every six years was proposed.

Denoon et. al [3] [4] and Denoon [5] conducted experiments in three airport towers equipped with accelerometers and anemometers. With help of the test it was concluded that the average threshold of perception varied with the natural frequency of the building. It is noteworthy that even though two of the buildings experienced accelerations that were acceptable according to the ISO 6897:1984 [6] which applied back then, one of the buildings received more complaints. It is believed that the tower was exposed to winds during a longer period of time, suggesting that exposure duration affects the perception of vibration. This is an important consideration, since the characteristics of windstorms differ greatly across the world.

Recently Lamb et al. [7] conducted surveys of 47 office workers in 22 buildings with a control group of 53 workers. The study was performed in Wellington, New Zealand, a notoriously windy city. With a risk of earthquakes in the country, designers are forced to allow for more structural flexibility which makes buildings more prone to dynamic response. 1909 surveys were collected during an eight month period and investigated. It was noted that there is a significant increase amongst the workers experiencing nausea and dizziness when building motion was possibly or definitely perceivable as shown in Figure 2.1.

When asked to rate their own work performance there was a clear indication that work-

ers in a higher Combined Motion Sickness Scale (CMSS) score group experienced a drop in their overall work performance, shown in Figure 2.2.

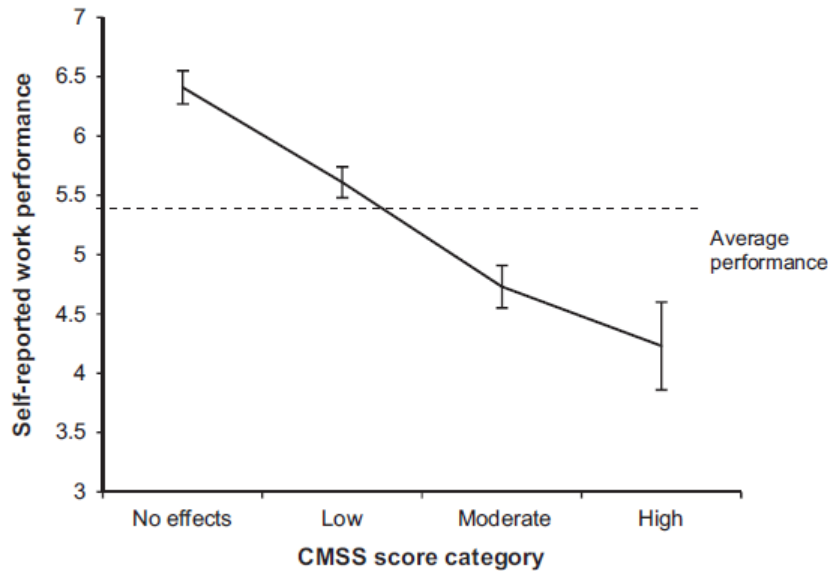


Figure 2.2: Work performance in the study [7]

The study showed that 60–70% of the participants detected building motion by vestibular or proprioceptive cues, i.e by feeling the sensation of motion. 12–32% detected it by sound cues and approximately 10% due to visual cues. Symptoms such as nausea and dizziness did not differ significantly when motion was possible or definite, suggesting the accelerations that are barely or not even perceived might affect occupants. The research was somewhat limited since the maximum observed wind-speed was only 75% of the design wind-speed with a one-year return period, but still shows the impact of buildings dynamic response can have on its users.

2.1.2 Motion simulators and shaker table experiments

To circumvent the uncertainties associated with field experiment a series of controlled motion simulators and shaker table experiments have been performed. The early experiments focused on participants subjected to sinusoidal vibrations and focused on vibrations perception without the subject being distracted by a task. Even though this may not be a realistic comparison to random wind-induced building vibration, some conclusion drawn still hold interest. One of the most referenced study to date is by Chen and Robertson [8] which concluded that the frequency of oscillation, body movement and expectancy of vibrations are factors that in large degree affect subjects vibration perception threshold.

Goto [9] performed vibration threshold experiments in the frequency range 0.1–1.0 Hz and showed that females have a lower threshold than males and adults lower than children. It was also shown that the threshold was lower for fore-aft vibrations than lateral and that standing lowered the threshold compared to being seated.

Irwin [10] conducted experiments on subjects exposed to yaw vibrations in the range between 0.05 and 5 Hz. Apart from the study showing a significant discrepancy in yaw acceleration threshold among individuals, the lowest being 0.001 rad/s^2 and the highest being 0.8 rad/s^2 , it also showed that the presence of a window in the testroom lowered the perception threshold.

Irwin and Goto [11] continued the study by Irwin and concluded that frequencies below 1 Hz resulted in more nausea and abdominal discomfort while frequencies above 1 Hz were more disturbing when subjects tried to perform manual tasks. As noted by Wong et al. [12] none of the tasks performed in the study are common in a modern office building, but experiments which more suit the modern environment show that task performance does decrease with increasing accelerations.

A comprehensive study by Burton et al. [13] on more than 500 subjects revealed that subjects are more likely to experience discomfort and nausea when subjected to a normally distributed waveform compared to a sinusoidal waveform. During the tests it was noted that subjects exposed to the vibrations for a longer period of time, 50 minutes instead of 12 minutes, was more likely to experience discomfort.

2.2 Recommendations and codes

With data gathered from some of the studies mentioned above led to the development of ISO 6897:1987 [6]. The limits were set at the maximum standard deviation of acceleration from the worst 10 minutes of windstorms occurring every 5 years.

The standard was later modified by Melbourne and Cheung [14] to specify a peak acceleration instead of the mean deviation used in ISO 6897:1987. Similar to the ISO the acceleration criteria depends on frequency and was given for different return periods. The recommendations can be found in Figure 2.3.

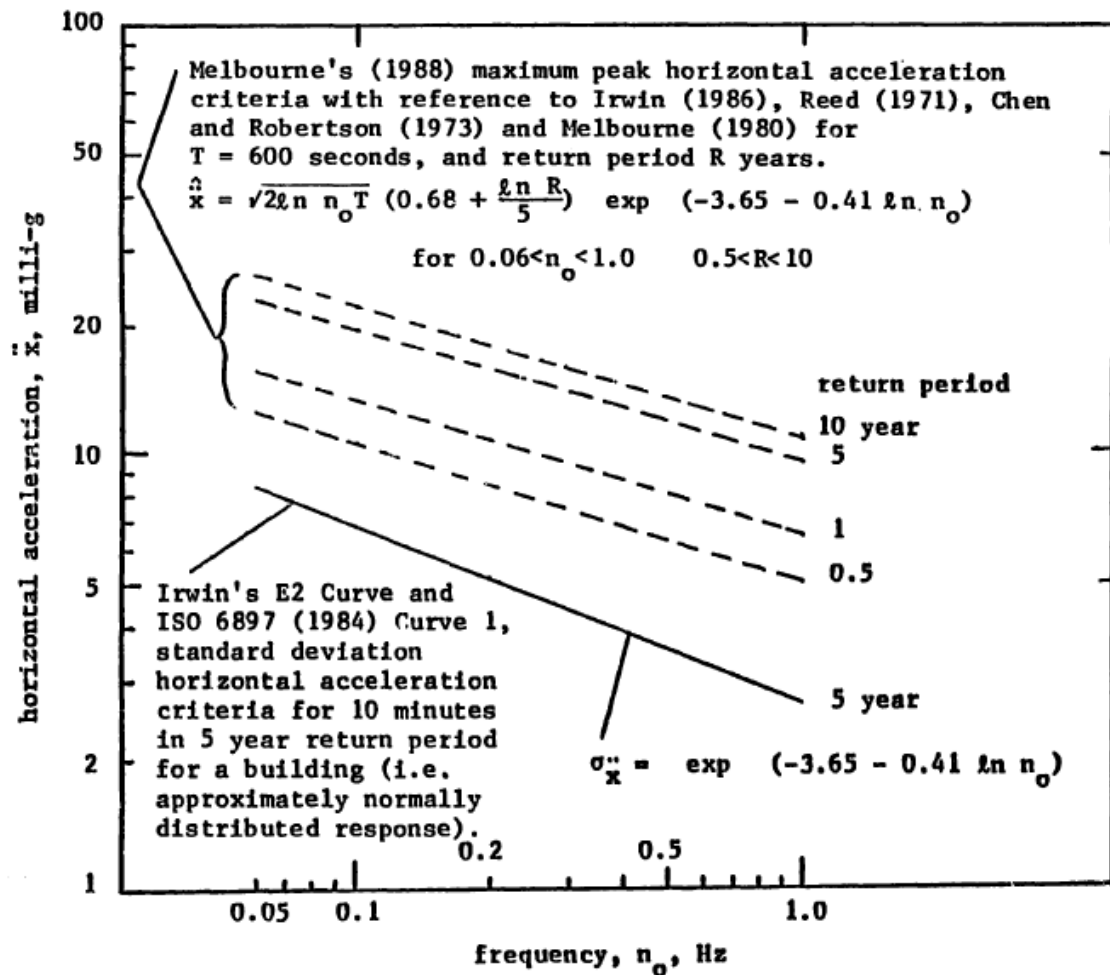


Figure 2.3: Proposed acceleration by Melbourne and Palmer [15].

In 1993 Isyumov [16] suggested ranges of accelerations which were incorporated in the National Building Code of Canada (NBCC) [17] in the 1995 edition. Instead of a frequency dependent criteria, intervals were suggested depending on the buildings usage, 5–7 mg for residential, 7–9 mg for hotels and 9–12 mg for offices [18]. The Architectural Institute of Japan (AIJ) [19] have gone in another direction. Instead of giving thresholds for human comfort the acceleration for a 10, 30, 50 70 and 90% probability of perception has been suggested. This lets owners decide for themselves what accelerations at an annual return period can be considered acceptable. The perception curves can be found in Figure 2.4.

ISO 6897:1984 [6] has later been revised and superseded by ISO 10137:2008 [21]. The acceptability curve for resident buildings lies close to that of AIJ's 90% probability curve. The criteria for resident buildings is 2/3 of that acceptable in offices. Figure 2.5

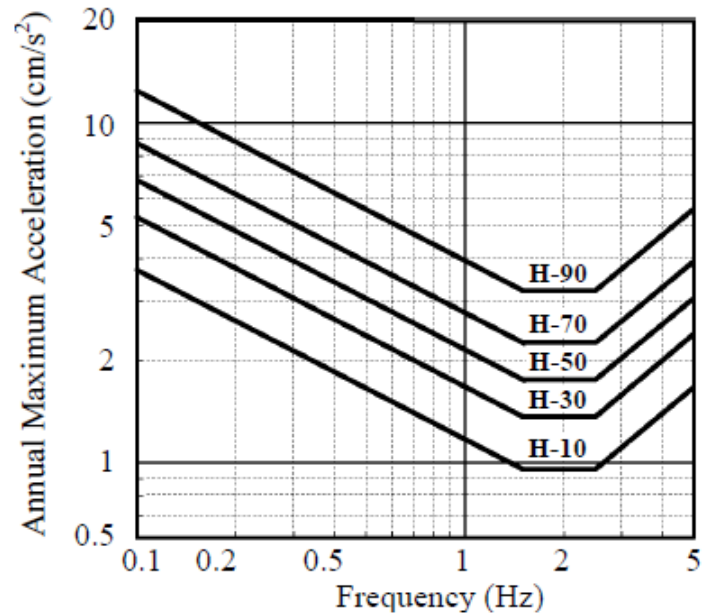


Figure 2.4: Probability of perception-curves used in AIJ [20].

shows the proposed criteria with the first line being suggested for offices and the second for residential buildings. A number of proposed criteria and perception thresholds have been summarised by Burton et al. [18] and are shown in Figure 2.6.

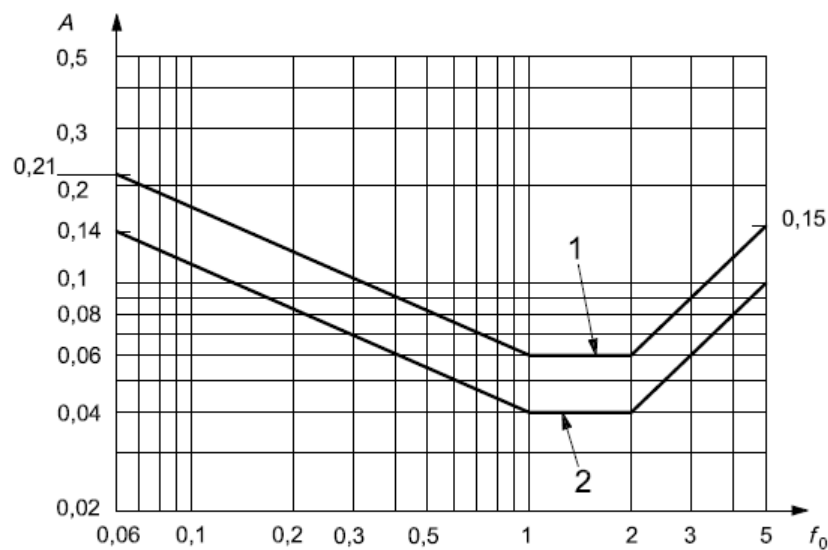


Figure 2.5: Acceptable accelerations according to ISO 10137:2008 [21].

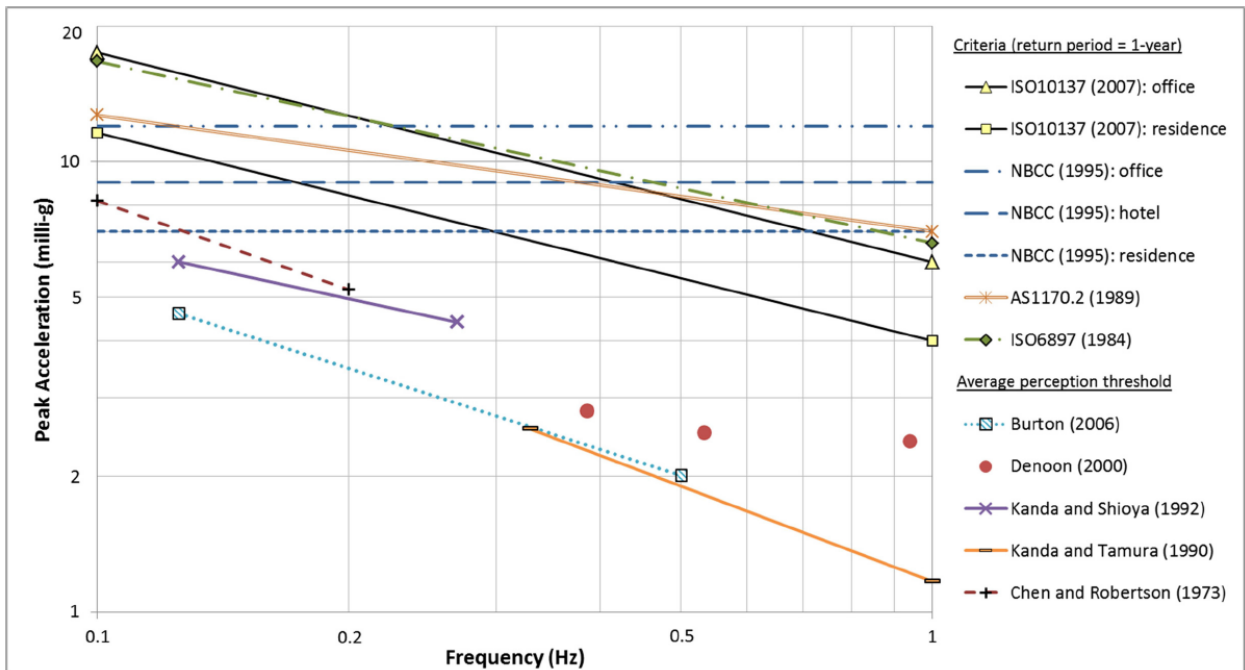


Figure 2.6: Proposed criterion and perception curves summarised by Burton et al. [18].

2.3 Wind tunnel testing

One major step forward in wind engineering was the development of the boundary layer wind tunnel. While many different test set-ups are available, one of the most common is the High Frequency Force Balance (HFFB) method. A rigid foam model with a high natural frequency is placed on a sensitive five-component balance. By performing several test, a average response spectrum of the base bending moment is obtained. The response spectrum is only valid for the particular building shape and environmental exposure tested, while being normalised to be independent of wind velocity and structural parameters such as stiffness, damping and mass [22]. Figure 2.7 shows the basic setup of a balance model.

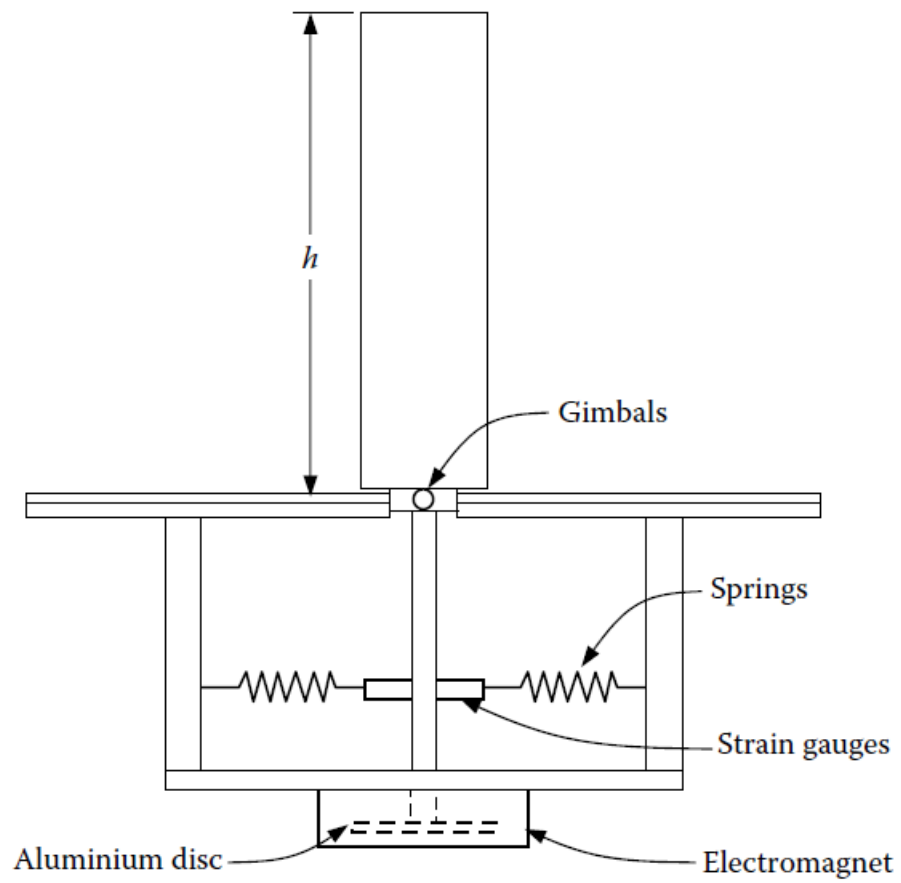


Figure 2.7: A base-pivoted building model used for HFFB testing. [23].

3. Acceleration formulas

Since serviceability criteria are often harder to fulfil than the survivability ones, it is of interest at an early stage in the design phase to have some sort of indication of a building's acceleration response. The Eurocode does provide some expressions for calculating a peak acceleration in the along-wind direction. However, the guidelines are only valid up to 200 meters and no expression for calculating the across-wind response is available. This chapter aims to slightly modify the existing Eurocode formulas while also giving an expression for estimating across-wind accelerations.

3.1 Along-wind response

The Eurocode allows for the accelerations to be determined by two different procedures, called Procedure 1 and Procedure 2. As shown by Steenbergen et al. [24] both procedures are based on the work of Davenport [25] but use different simplifications. Due to the simplifications made procedure 2 is deemed better at estimating accelerations in tall and slender buildings. The equation for the standard deviation of the characteristic along-wind acceleration is written as

$$\sigma_{a,x}(y,z) = c_f \cdot \rho \cdot I_v(z_s) \cdot v_m^2(z_s) \cdot R \cdot \frac{K_y \cdot K_z \cdot \phi(y,z)}{\mu_{ref} \cdot \phi_{max}} \quad (3.1)$$

where:

c_f is the force coefficient

ρ is the air density

$I_v(z_s)$ is the turbulence intensity at height z_s above ground

$v_m(z_s)$ is the characteristic mean wind velocity at height z_s

z_s is the reference height

R is the square root of the resonant response

K_y, K_z are constants given in Eurocode

μ_{ref} is the reference mass per unit area

$\phi(y, z)$ is the mode shape

ϕ_{max} is the mode shape value at the point with maximum amplitude

As shown in a comparative study by Kwon and Kareem [26] all major international codes are based on the same random-vibration-based gust loading factor approach. By comparing the individual components of Equation 3.1 with those of other international codes an equation estimating the accelerations in buildings taller than 200 meters might be proposed.

c_f Force coefficient

The force coefficient, see (c_f . Equation 3.2), is the absolute sum of the windward and leeward pressure coefficients. Pressure coefficient in Eurocode are given for a height to depth ratio of maximum 5, ie $h/d < 5$. For buildings that do not satisfy this condition, the force coefficient can be calculated according to Section 7.6 in the Eurocode. The force coefficient is expressed as

$$c_f = c_{t,0} \cdot \psi_r \cdot \psi_\lambda \quad (3.2)$$

where c_t for rectangular sections with sharp corners are given by Figure 3.1. ψ_r is a reduction factor for rectangular shapes with rounded corners. These values are given by Figure 3.2. The end effect factor ψ_λ is given by Figures 3.3 and 3.4. ϕ in Figure 3.4 is equal to 1 for cladded structures. The force coefficient can vary extensively when a tall building is surrounded by other buildings. In these cases the force coefficient is best determined by wind-tunnel testing.

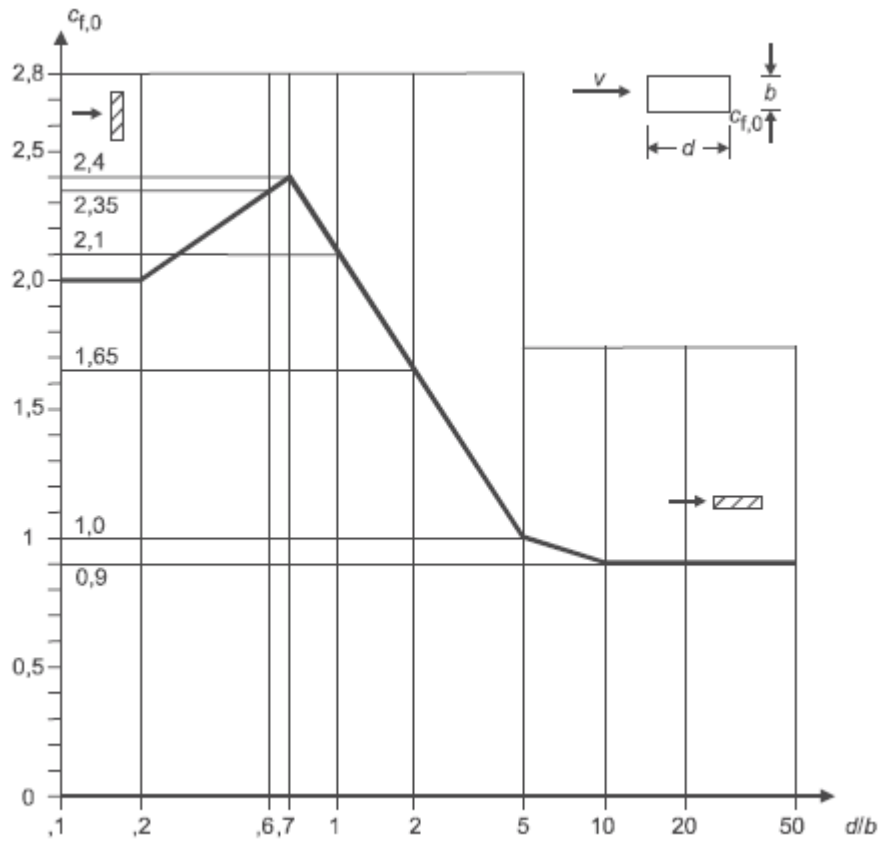


Figure 3.1: $c_{f,0}$ as a function of a rectangular cross-section.

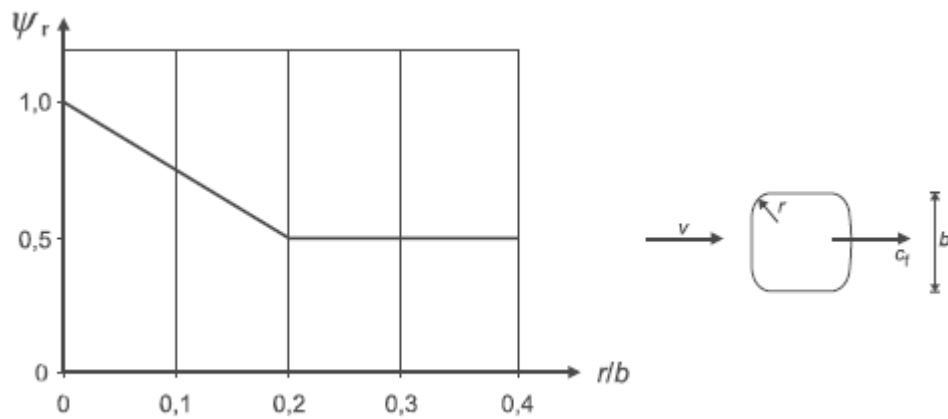


Figure 3.2: Reduction factor ψ_r for rounded corners.

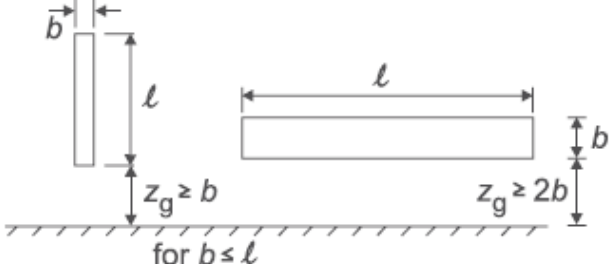
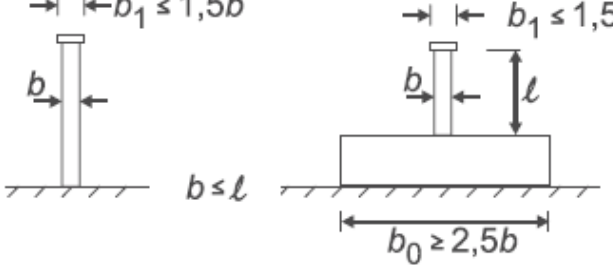
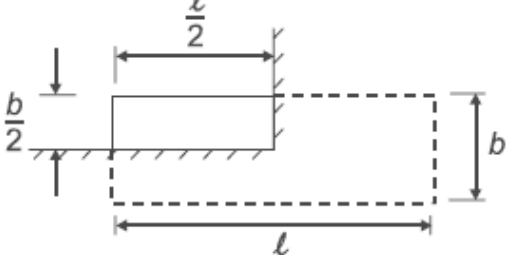
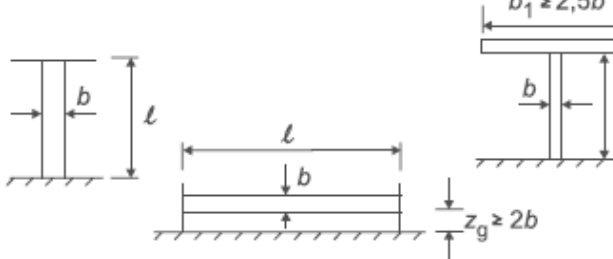
No.	Position of the structure, wind normal to the plane of the page	Effective slenderness λ
1		<p>For polygonal, rectangular and sharp edged sections and lattice structures:</p> <p>for $\ell \geq 50$ m, $\lambda = 1,4 \ell/b$ or $\lambda = 70$, whichever is smaller</p>
2		<p>for $\ell < 15$ m, $\lambda = 2 \ell/b$ or $\lambda = 70$, whichever is smaller</p> <p>For circular cylinders:</p> <p>for $\ell \geq 50$, $\lambda = 0,7 \ell/b$ or $\lambda = 70$, whichever is smaller</p> <p>for $\ell < 15$ m, $\lambda = \ell/b$ or $\lambda = 70$, whichever is smaller</p>
3		<p>For intermediate values of ℓ, linear interpolation should be used</p>
4		<p>for $\ell \geq 50$ m, $\lambda = 0,7 \ell/b$ or $\lambda = 70$, whichever is larger</p> <p>for $\ell < 15$ m, $\lambda = \ell/b$ or $\lambda = 70$, whichever is larger</p> <p>For intermediate values of ℓ, linear interpolation should be used</p>

Figure 3.3: Recommended slenderness values.

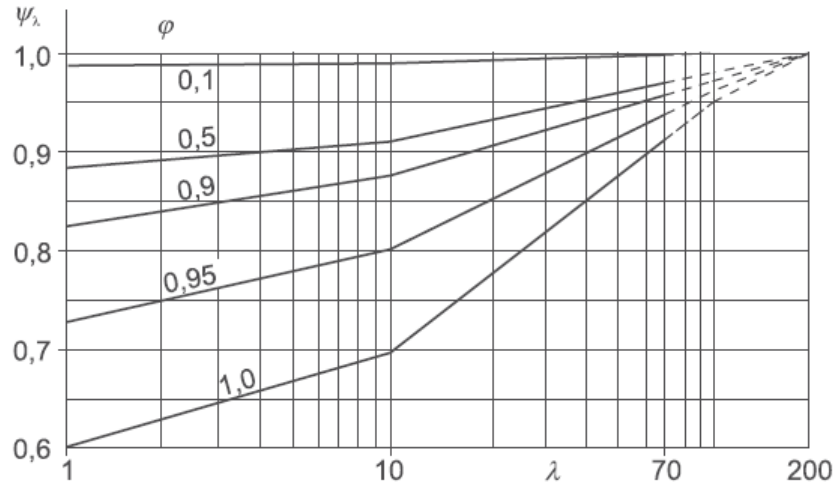


Figure 3.4: Reduction factor of force coefficient for structural elements with end-effects ψ_λ .

ρ Air density

The air density ρ is set to 1.25 kg/m^3 but with the decreasing temperature further up in the atmosphere, the density drops. In international codes a more common value of 1.22 kg/m^3 is adopted.

I_v Turbulence intensity

The turbulence intensity is described as

$$I_v(z) = \frac{k_l}{c_o(z) \cdot \ln(z/z_0)} \quad (3.3)$$

Where k_l is the turbulence factor. This might be given in a National Annex, but the recommended value is 1. c_o is an orography factor which in flat environment may be taken as 1. This reduces the expression to

$$I_v(z) = \frac{1}{\ln(z/z_0)} \quad (3.4)$$

where z_o is the roughness length, which depends on the terrain and is given by Table 4.1 in the Eurocode. z is the height above ground. A majority of international codes instead of a logarithmic law uses a power law to describes the turbulence. This can be written as

$$I_v(z) = c \left(\frac{10}{z} \right)^d \quad (3.5)$$

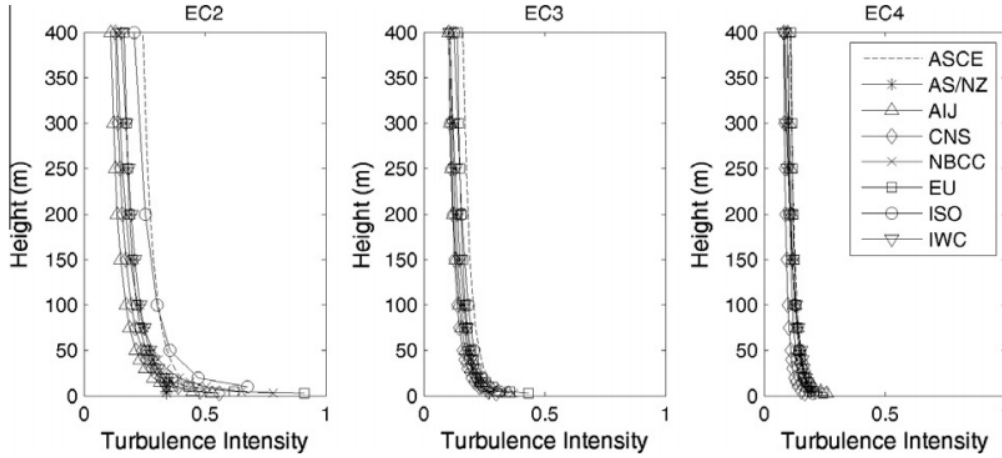


Figure 3.5: Turbulence intensity profiles for different terrain categories and international codes [26].

where c and d have different values depending on the terrain. Kwon et al. [26] showed that the power law gives a lower turbulence intensity, especially for rougher terrain categories. The difference in turbulence intensity calculated using international codes are shown for three exposure classes in Figure 3.5. EC2 corresponds to Eurocode's terrain category IV and EC4 to II. Using a power law has the advantage that it is easy fitted to measured data. It should also be noted that codes use different heights z to calculate the turbulence intensity. A majority of codes use the actual height of a building, whereas Eurocode and the ASCE (American Society of Civil Engineers) use $0.6h$ where h is the height of the building. Since the turbulence is greatly influenced close to the ground but becomes more steady on higher altitudes, the choice of reference height does not have a large impact on the turbulence.

v_m^2 Characteristic mean wind velocity

The characteristic mean wind velocity v_m^2 is expressed as

$$v_m(z) = c_r(z) \cdot c_0(z) \cdot v_b \quad (3.6)$$

where $c_r(z)$ is the roughness factor, c_0 the orography factor and v_b the basic wind velocity. The orography factor is often set to 1, while the roughness factor depends on the terrain category. The roughness factor is expressed as

$$c_r(z) = k_r \ln \left(\frac{z}{z_0} \right) \quad z_{min} < z < z_{max} \quad (3.7)$$

where

$$k_r = 0.19 \cdot \left(\frac{z_0}{z_{0,II}} \right)^{0.07} \quad (3.8)$$

and z_{max} is 200 meters. As with the turbulence intensity many international codes instead use a power law to describe the mean wind velocity. The expression is described as

$$v_m(z) = b \left(\frac{z}{10} \right)^\alpha v_b \quad (3.9)$$

where b and α are factors that depend on the terrain category. Appropriate α and b values are for different terrain categories are given by Kwon et al [26]. Note that there are still large discrepancies how codes define α and b , especially for urban environments. Proper values should be decided by wind-tunnel testing. The power-law can also generally be expressed without the b -factor and can then be fitted to the logarithmic law with the expression

$$\alpha = \left(\frac{1}{\log_e(z_{ref}/z_0)} \right). \quad (3.10)$$

Resonant response

The resonant response factor allows for turbulence in the wind that coincide with the natural frequency for a vibration mode in a building. It is expressed as a function of a size reduction factor K_s , an energy factor S_L and the damping of a building ζ .

$$R^2 = \frac{\pi^2}{2 \cdot \zeta} S_L(z_s, n_{1,x}) \cdot K_s(n_{1,x}). \quad (3.11)$$

Values for ζ are given in Annex F5 of the Eurocode. S_L is the variance spectrum describing how the variance of the stochastic wind is distributed over different frequencies. Eurocode use the Kaimal spectral density function which is expressed as

$$S_L = \frac{n \cdot S_v(z, n)}{\sigma_v^2} = \frac{6.8 \cdot f_L(z, n)}{(1 + 10.2 \cdot f_L(z, n))^{5/3}} \quad (3.12)$$

and is the non-dimensional frequency and n is the natural frequency for the lowest mode of the building. v_m has been expressed in Section 3.1. $L(z)$ is the turbulent length scale which represents the average gust size for natural wind. This is expressed as

$$\begin{aligned} L(z) &= L_t \cdot \left(\frac{z}{z_t} \right)^\alpha & \text{for } z > z_{min} \\ L(z) &= L(z_{min}) & \text{for } z < z_{min} \end{aligned} \quad (3.13)$$

with $z_t = 200$ meters and the reference length scale $L_t = 300$ meters and $\alpha = 0.67 + 0.05 \cdot \ln(z_0)$ where z_0 is the roughness length which depends on the terrain category.

As mentioned in Sharpe et al. [27] recent studies suggest that the von Karman spectrum gives a better representation of turbulence above 150 meters. The von Karman spectrum is used in major codes such as AS/NZ, AIJ, ISO and IWC. The von Karman spectrum is expressed as

$$S_L = \frac{4 \cdot f_L(z, n)}{(1 + 71.8 f_L(z, n)^2)^{5/6}}. \quad (3.14)$$

According to the Kolmogorov law, both spectrum must approach the asymptotic limit proportional to $n^{-5/3}$ for higher frequencies. This results in different turbulence length for the two spectra. According to AIJ the turbulence length for the Karman spectrum can be described as

$$L(z) = 100 \cdot \left(\frac{z}{30}\right)^{0.5} \quad \text{for} \quad 30m < z < z_g \quad (3.15)$$

$$L(z) = 100 \quad \text{for} \quad z < 30m$$

where z_g is determined by the terrain category and is shown in Table 3.1.

Table 3.1: Height limit according to AIJ

Category	I	II	III	IV	V
z_g (m)	250	350	450	550	650

Depending on the surface roughness the turbulence is no longer influenced by the ground, i.e the turbulence length remains equal above this height. This boundary height is expressed as

$$z_i = 1000z_0^{0.18} \quad (3.16)$$

where z_0 is the surface roughness. The turbulence length up to that level can be expressed as

$$L(z) = 280 \cdot \left(\frac{z}{z_i}\right)^{0.35}. \quad (3.17)$$

$K_s(n_{1,x})$ is the size reduction factor expressed as

$$K_s(n_{1,x}) = \frac{1}{1 + \sqrt{(G_y \cdot \phi_y)^2 + (G_z \cdot \phi_z)^2 + \left(\frac{2}{\pi} \cdot G_y \cdot \phi_y \cdot G_z \cdot \phi_z\right)^2}} \quad (3.18)$$

where

$$\phi_y = \frac{c_y \cdot b \cdot n}{v_m(z_s)} \quad \phi_z = \frac{c_z \cdot b \cdot n}{v_m(z_s)}. \quad (3.19)$$

The constants c_y and c_z are equal to 11.5 while n is the natural frequency for the mode shape. For uniform, linear, parabolic and sinusoidal mode shapes G and K can be found in Table 3.2

Table 3.2: G and K as a function of mode shape

Modeshape	Uniform	Linear	Parabolic	Sinusoidal
G:	1/2	3/8	5/18	$4\pi^2$
K:	1	3/2	5/3	$4\pi^2$

Since accelerations at the top of a building often is desired the expression

$$\frac{K_y \cdot K_z \cdot \phi(y, z)}{\phi_{max}} \quad (3.20)$$

becomes 1.5, assuming a linear vertical mode shape and a uniform horizontal one. According to Dyrbye and Hansen [28], K_y and K_z provides correct values when compared to the unsimplified theoretical expression.

Having calculated the standard deviation of along-wind acceleration ($\sigma_{a,x}$), the peak response (\hat{a}) can be obtained by multiplying with a peak factor (g_R).

$$g_R = \sqrt{2 \ln(600 f_1)} + \frac{0.5772}{\sqrt{2 \ln(600 f_1)}} \quad (3.21)$$

$$\hat{a}(z) = g_R \cdot \sigma_{a,x}(z) \quad (3.22)$$

The expression above with the changes discussed should provide designers with a preliminary acceleration response that can be used at an early stage of structural design.

3.2 Across-wind response

With tall and slender buildings, the across-wind response is often bigger than the along-wind response, due to vortex shedding will be described in Section 4. Since no theoretically derived expressions for estimating the across-wind exists, data from wind-tunnel testing has to be used instead. Some international building codes provide acceleration estimates in the across-wind direction. However, these are often restricted to buildings that are not very slender and where the response might not be dominated by dynamic resonance.

Quan and Gu

While the Eurocode does provide some calculation for estimating accelerations in the along-wind direction, none are given for across-wind. The AIJ provides expressions for determining the across-wind acceleration for buildings which satisfies the following conditions

$$\begin{aligned}\frac{H}{\sqrt{BD}} &\leq 6 \\ 0.2 &\leq \frac{D}{B} \leq 5 \\ \frac{U_H}{f_L \sqrt{BD}} &\leq 10\end{aligned}$$

where H , B and D are the height, breadth and depth in meters respectively of the building. Furthermore U_H is the reference wind-speed (m/s) at the top of the building and f_L the fundamental frequency (Hz).

As pointed out by Kwon et al. [29] the empirical expressions for the spectrum in AIJ are not a function of boundary layer condition, terrain or building height. Gu and Quan [30] performed a number of wind tunnel experiments and described the spectrum as a function of parameters mentioned. A 60 cm aerolastic model represents a 300 meter high building. Wind tunnel test were performed on models with a breadth-to-depth ration of 0.33 to 3 and height-to-base ratios of 1 to 8. Using this a method more suited for estimating acceleration in taller and slender buildings was developed. The method is described hereafter. First the structural and geometric parameters are obtained. These include the building height H , breadth B , depth D , first natural frequency in the across-wind direction f_1 , mode shape β , structural damping ζ_s and the mass $m(z)$ per unit height. With these parameters the first generalized mass can be calculated using

$$M_i^* = \int_0^H m(z) \cdot \phi_i^2(z) dz \quad (3.23)$$

Furthermore, parameters such as wind field exponent α , turbulence intensity I_H , wind speed U_H and wind pressure w_H at the building height H are obtained. The parameters are used to calculate the background base moment coefficient as

$$C_{M\beta 0} = 0.182 - 0.019\alpha_{db}^{-2.54} + 0.054\alpha_w^{0.91} \quad (3.24)$$

where α_{db} is the breadth to width ratio and α_w a terrain coefficient, both which are defined in Equation 3.30. Similar to the gust loading model, a peak factor (g_R of the resonant response is needed.

$$g_R = \sqrt{2\ln(600f_1)} + \frac{0.5772}{\sqrt{2\ln(600f_1)}} \quad (3.25)$$

Where f_1 (Hz) is the first natural frequency of the building. Furthermore a mode shape correction factor is needed since the High Frequency Force Balance (HFFB) method use a structure with an idealised mode shape as

$$\Phi = \begin{cases} (4\alpha + 3)/(4\alpha + 2\beta + 1) & \beta \leq 1.0 \\ [(2\alpha + 2)/(2\alpha + \beta + 1)]^2 & \beta \geq 1.0. \end{cases} \quad (3.26)$$

When the mode shape is linear, β is set to 1. α is the wind profile exponent described in Equation 3.9.

The aerodynamic damping ratio is approximated by

$$\zeta_a = \frac{0.0025 (1 - (U^*/9.8)^2) (U^*/9.8) + 0.000125(U^*/9.8)^2}{(1 - (U^*/9.8)^2)^2 + 0.0291(U^*/9.8)^2} \quad (3.27)$$

Where U^* is the reduced wind speed at the top of the building, $U^* = U_H(f_1/B)$. The spectral density of the base bending moment is described by

$$S_M^*(f_1) = \frac{S_P \beta (f_L/f_p)^2}{(1 - (f_L/f_p)^2)^2 + \beta (f_L/f_p)^2} \quad (3.28)$$

Where f_p , S_p , β and α are parameters used to fit the expression to test data from wind tunnel tests.

$$f_p = 10^{-5} (191 - 9.48\alpha_w + 1.28\alpha_{hr} + \alpha_{hr}\alpha_w) (68 - 21\alpha_{db} + 3\alpha_{db}^2)$$

$$S_P = (0.1\alpha_w^{-0.4} - 0.0004e^{\alpha_w}) (0.84\alpha_{hr} - 2.12 - 0.05\alpha_{hr}^2) (0.422 + \alpha_{db}^{-1} - 0.08\alpha_{db}^{-2})$$

$$\beta = (1 + 0.00473e^{1.7\alpha_w}) (0.065 + e^{1.26 - 0.63\alpha_{hr}}) e^{1.7 - 3.44/\alpha_{db}}$$

$$\alpha = (-0.82 + 0.06\alpha_w + 0.0007e^{\alpha_w}) (-\alpha_{hr}^{0.34} + 0.00006e^{\alpha_{hr}}) (0.414\alpha_{db} + 1.67\alpha_{db}^{-1.23}) \quad (3.29)$$

where

$$\begin{aligned} \alpha_{hr} &= H/\sqrt{BD} \\ \alpha_{db} &= D/B \\ \alpha_w &= \begin{cases} 1 & (A) \\ 2 & (B) \\ 3 & (C) \\ 3 & (D). \end{cases} \end{aligned} \quad (3.30)$$

α_w represents different terrain categories with mean wind velocity power-law exponents of 0.12, 0.16, 0.22 and 0.30, respectively. The corresponding gradient heights are 300, 350, 400 and 450 meters, respectively.

Using the equations above an acceleration at the height z can be calculated.

$$\hat{a}(z) = \frac{H}{M_1^*} B_{GRWH} \left(\frac{z}{H}\right)^\beta \cdot \sqrt{\frac{\pi \Phi S_M^*(f_1)}{4(\zeta_{s1} + \zeta_{a1})}} \quad (3.31)$$

The expressions above give designers an estimate of a building's dynamic response in the early design stages. Once the final design has been decided, wind-tunnel testing might prove necessary to give further insight in the dynamic behaviour of the building.

4. Numerical modelling and simulations

This chapter discusses numerical modelling and simulation of a building subjected to wind load. Some basic theory about wind-loading, followed by how the building has been modelled is described. An equivalent static wind-load was calculated and applied to the model. The static deflection was used to define two Ritz-vectors, one in each translational direction. The results between a large system and one reduced by Ritz-vectors in a 600 seconds long time-stepping analysis were compared.

Gust loading factor

The most common procedure when evaluating the response of a building was developed by Davenport in 1967 [25]. Using a gust loading factor G_Y , a peak response \hat{P} including dynamic amplification can be calculated from the mean response \bar{P} . The method can be used to calculate a number of responses, such as forces, accelerations and displacements. Using force as an example, the method in Holmes [23] is briefly described below.

$$\hat{P} = G_Y \cdot \bar{P} \quad (4.1)$$

Where G_Y is the gust loading factor. It is evaluated in terms of the relationship between the mean \bar{Y} and expected peak displacement \hat{Y}

$$G_Y = \hat{Y}(z)/\bar{Y}(z) \quad (4.2)$$

For a stationary process, G_Y is given by

$$G_Y = 1 + g_Y \sigma_Y(z)/\bar{Y}(z) = 1 + 2g_Y I_H \sqrt{B + R} \quad (4.3)$$

where

g_Y is the peak response factor.

$\sigma_Y(z)$ is the RMS displacement

B and R are the background and resonant response factor

I_H is the turbulence at the top of the building

Note that g_y has been used previously but divided in to a background and resonant part g_b and g_r .

Vortex shedding

Vortex shedding is a phenomenon that has high impact on acceleration levels in tall and slender buildings. Due to their often bluff body, oncoming wind is shed alternately on each side of the building, resulting in a force acting perpendicular to the wind.

The Eurocode gives the critical velocity where the vortex shedding frequency coincides with the natural frequency of a building. The critical velocity can be described as

$$v_{crit} = \frac{b \cdot n}{St} \quad (4.4)$$

where

b (m) is the breadth of the building perpendicular to the oncoming wind.

n (Hz) is the natural frequency of the building.

St is the Strouhal number, defined by Figure 4.1.

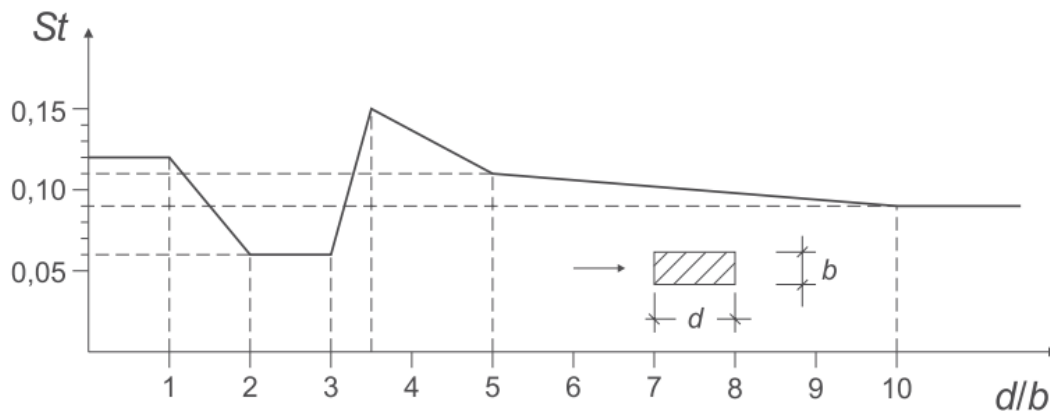


Figure 4.1: Strouhal number for rectangular cross-sections with sharp corners

Since the shedding frequency often lies close to the fundamental frequency of tall buildings, a dynamic amplification can result in very high acceleration levels due to resonance.

Modelled building

Modelling of the building is done in MATLAB using CALFEM, a finite element toolbox developed at Department of Construction Sciences at Lund University. The code can be found in appendixes. The *main.m* file contain the main program which generates the mass and stiffness matrix for an idealised building. The weight of the building is equally distributed to the nodal points. The stiffness is adjusted to provide a first natural frequency close to that of tall buildings. A common rule for determining the lowest natural frequency of a tall buildings is $46/H$.

The *TimeSeries.m* file creates a target spectrum in the along- and across wind direction. An Inverted Fast Fourier Transform (IFFT) routine is performed to generate two time-series. Finally a Fast Fourier Transform (FFT) analysis on the time-series if performed to confirm that the generated time-series include the same frequencies as the target spectrum.

The *EWSL.m* file generates the equivalent static wind-load used by the main program to calculate a static deflection which later on is used as a Ritz-vector to reduce the system.

A building with 85 floors and a rectangular cross-section of $50 \times 50 \text{ m}^2$ is shown in Figure 4.2. The building has a floor height of 3.5 meters and a total height of 297.5 meters. The density is set to 180 kg/m^3 which is equally distributed to the translational degrees of freedom. A small mass is added to the rotational degrees of freedom to avoid numerical errors. The lowest natural frequency is 0.1574 in the translational directions. The total system consists of 3360 number of nodes and 8160 degrees of freedom. It is modelled using three dimensional beam elements with rigid connections.

The damping-matrix, \mathbf{c} , is determined using Rayleigh damping using the mass matrix \mathbf{m} and stiffness matrix \mathbf{k} . [31]

$$\mathbf{c} = a_0 \mathbf{m} + a_1 \mathbf{k} \quad (4.5)$$

where

$$\begin{aligned} a_0 &= \zeta \frac{2\omega_1 \omega_2}{\omega_1 + \omega_2} \\ a_1 &= \zeta \frac{2}{\omega_1 + \omega_2}. \end{aligned} \quad (4.6)$$

With a structural damping of 1% [32] and first and second translational frequencies as 0.1574 Hz and 0.4777 Hz, the factors a_0 and a_1 becomes 0.003 and 0.13, respectively.

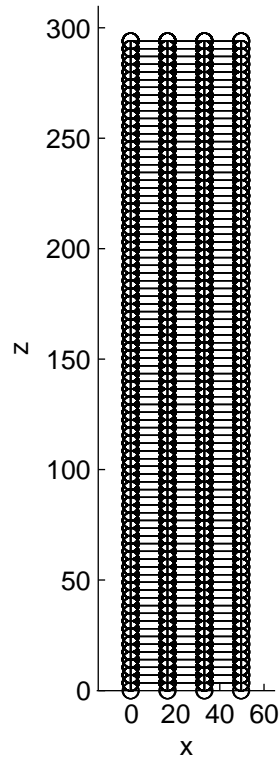


Figure 4.2: Structure modelled in CALFEM with dimensions in meters.

4.1 Ritz vectors

The following section gives a brief overview on the use of Ritz-vectors. The theory is described in Chopra [31].

The usual equation of motions for a multi-degree-of-freedom (MDOF) system with N dofs can be written as

$$m\ddot{\mathbf{u}} + \mathbf{c}\dot{\mathbf{u}} + \mathbf{k}\mathbf{u} = \mathbf{p}(t) \quad (4.7)$$

where \mathbf{m} , \mathbf{c} , and \mathbf{k} are the mass-, damping- and stiffness-matrix respectively. \mathbf{u} , $\dot{\mathbf{u}}$ and $\ddot{\mathbf{u}}$ are the displacement, velocity and acceleration vectors. $\mathbf{p}(t)$ is a vector that contains the external force applied in each degree of freedom.

By selecting a number of Ritz vectors, representing expected mode shapes, a large system can be reduced, thus saving computational time. For example, choosing a

single Ritz-vector results in a single-degree-of-freedom (SDOF) system.

$$\mathbf{u} \approx \sum_{i=1}^J z_i(t) \Psi_i = \Psi \mathbf{z}(t). \quad (4.8)$$

Substituting this into the original equation gives

$$\mathbf{m} \Psi \ddot{\mathbf{z}} + \mathbf{c} \Psi \dot{\mathbf{z}} + \mathbf{k} \Psi \mathbf{z} = \mathbf{p}(t). \quad (4.9)$$

Furthermore, premultiplying with Ψ^T gives

$$\tilde{\mathbf{m}} \ddot{\mathbf{z}} + \tilde{\mathbf{c}} \dot{\mathbf{z}} + \tilde{\mathbf{k}} \mathbf{z} = \tilde{\mathbf{p}}(t). \quad (4.10)$$

This gives a reduced system where

$$\tilde{\mathbf{m}} = \Psi^T \mathbf{m} \Psi, \quad \tilde{\mathbf{c}} = \Psi^T \mathbf{c} \Psi, \quad \tilde{\mathbf{k}} = \Psi^T \mathbf{k} \Psi, \quad \tilde{\mathbf{p}} = \Psi^T \mathbf{p}. \quad (4.11)$$

This gives a much smaller system with as many degrees of freedom as numbers of Ritz-vectors used to reduce the system. Once the matrices have been reduced the dynamic analysis can be performed with time-stepping methods. The reduced system response can be transformed back to the original response variable. For example, the accelerations in the full system can be retrieved using Equation 4.10 giving

$$\ddot{\mathbf{u}} = \Psi \ddot{\mathbf{z}}. \quad (4.12)$$

Since the same vectors have been used to scale the system, the final matrices will be the same size as the original ones. This means that even though the system was reduced to a few dofs, any degree of freedom can be observed once the reduced response has been transformed back to its original form.

If a good the choice of Ritz-vectors was made, the system can be solved with high accuracy. One way of determining the Ritz-vectors is by having a physical insight to the building's behaviour. While this may be suitable for simpler systems, such as shear buildings, estimating mode shape for buildings with a higher number of dofs may be more difficult. Another way of determining the Ritz-vectors is by applying an equivalent static average wind-load and using the calculated deflection as a Ritz-vector.

4.2 Equivalent static wind-load

To determine the Ritz-vectors, a static deflection was calculated. To do this the structure was subjected to a static wind-load. The sections below describe how the load was determined.

Along-wind

The Eurocode does not provide a method of determining the equivalent static wind load (ESWL) for a building. Instead a method for determining the ESWL in the along-wind direction has been developed by Zhou et al. [33]. The method is based on the principle of a gust loading factor originally developed by Davenport and is more suitable for taller and more slender buildings. The method is described below.

First of, the mean wind-force \bar{P}_i on each level is calculated.

$$\bar{P}_i = \left(\frac{1}{2} \rho \bar{U}_H^2 (Z_i/H)^{2\alpha} C_D (W \cdot \Delta H_i) \right) \quad (4.13)$$

with

- ρ Air density.
- \bar{U}_H^2 Mean wind speed at the building height H .
- Z_i Height above ground for floor i .
- H Building height.
- α Wind exponent factor.
- C_D Drag coefficient.
- W Width of building perpendicular to the oncoming wind.
- ΔH_i Floor height.

From this the total base bending moment (BBM) is calculated.

$$\bar{M} = \sum_{i=1}^N \bar{P}_i Z_i. \quad (4.14)$$

Following the procedure in any current building code the background response B_r , size reduction S and energy factor E are retrieved and the gust loading factor calculated. g_b and g_r are peak factors while I_H is the turbulence intensity at the top of the building and ζ_s the structural damping.

$$G_{MB} = 2g_b I_H \sqrt{B} \quad (4.15)$$

$$G_{MR} = 2g_r I_H \sqrt{SE/\zeta_s} \quad (4.16)$$

$$G_M = 1 + \sqrt{G_{MB}^2 + G_{MR}^2} \quad (4.17)$$

The resonant extreme base bending moment \hat{M}_R is calculated by multiplying the mean BBM \bar{M} with the gust loading factor G_{MR} for the resonant part.

$$\hat{M}_R = G_{MR} \bar{M}. \quad (4.18)$$

The background and resonant equivalent static wind-load for each floor can now be calculated. The resonant bending moment is simply distributed as loads on each floor. The background wind-load is calculated by multiplying the mean wind-load on each floor with the background gust loading factor.

$$\hat{P}_{Ri} = \frac{m_i \phi_i}{\sum m_i \phi_i Z_i} \hat{M}_R \quad (4.19)$$

$$\hat{P}_{Bi} = G_{MB} \bar{P}_i \quad (4.20)$$

Where m_i and ϕ_i is the floor mass and mode shape respectively. Adding the two gives the total equivalent static wind load on each floor.

Across-wind

As with along-wind loads, the Eurocode provides no means for calculation of the EWSL in the across-wind direction. While the AIJ may be suitable for common high-rise buildings, it is not suitable for very slender buildings where vortex shedding and a negative aerodynamic damping might have a significant impact on the building response. A method developed by Quan et al. [30] was used instead. The procedure is similar as described in Chapter 3.2 with some minor additions. The peak ESWL, $\tilde{p}(z)$, on each floor can be determined using

$$\hat{p}(z) = w_H B \sqrt{G_B^2(z) + G_R^2(z)} \quad (4.21)$$

where w_H is the wind pressure at the top of the building and

$$G_B(z) = (0.65 + 1.3z + 7z^2 - 7.5z^3) g_b C_{M-B0} \quad (4.22)$$

$$G_R(z) = \frac{Hm(z)}{M_1^*} \left(\frac{z}{H}\right)^\beta g_{R1} \sqrt{\frac{\pi \Phi S_M^*}{4(\zeta_{s1} + \zeta_{a1})}} \quad (4.23)$$

where all the parameters have been presented previously in Section 3.2.

4.3 Wind-load time series

For comparison between the full and reduced system a wind-load time-series has to be created. This section gives an overview of how it is generated.

Base moment spectrum

From wind-tunnel testing, the BBM is obtain in spectral form. In the across-wind direction the spectrum has already been described in Section 3.2 as S_M^* . In the along-wind direction it is described by AIJ as

$$\frac{fS_M(f)}{\sigma_M^2} = F_D \quad (4.24)$$

Where F_D is the along-wind force spectrum factor.

$$F_D = \frac{I_H^2 \cdot F \cdot S_D (0.57 - 0.35\alpha + 2R\sqrt{0.053 - 0.042\alpha})}{C_g'^2} \quad (4.25)$$

Where I_H is the turbulence intensity at the building height H , F is the wind spectrum force factor, S_D the size effect factor, α the wind speed exponent, R the factor expressing the correlation of wind pressure on the windward and leeward side and C_g' is the root-mean-square (RMS) overturning moment coefficient in the along-wind direction.

$$F = \frac{4 \cdot \frac{fL_H}{U_H}}{\left[1 + 71 \left(\frac{fL_H}{U_H}\right)^2\right]^{5/6}} \quad (4.26)$$

where f (HZ) is the first fundamental frequency of the building, L_H and U_H are the turbulence length scale and mean wind speed at height H .

$$S_D = \frac{0.9}{\left[1 + 6 \left(\frac{fH}{U_H}\right)^2\right]^{0.5} \left(1 + 3 \frac{fB}{U_H}\right)} \quad (4.27)$$

$$R = \frac{1}{1 + 20 \frac{fB}{U_H}} \quad (4.28)$$

$$C_g' = 2I_H \frac{0.49 - 0.14\alpha}{\left[1 + \frac{0.63(0.63\sqrt{BH}L_H)^{0.56}}{(H/B)^k}\right]} \quad (4.29)$$

$$k = \begin{cases} 0.07 & (H/B) \geq 1 \\ 0.15 & (H/B) < 1. \end{cases} \quad (4.30)$$

Using the spectrum an IFFT procedure with some added noise and random phase angle was performed, creating the time-series of the wind-load. By performing a FFT-analysis on the generated time-series, a spectral representation closely matches that of the closed form expression. Since no information is available regarding the original signal, the IFFT procedure has to be manually scaled. Figures 4.3 and 4.4 show examples of generated time-series and their spectral density compared to the target spectrum.

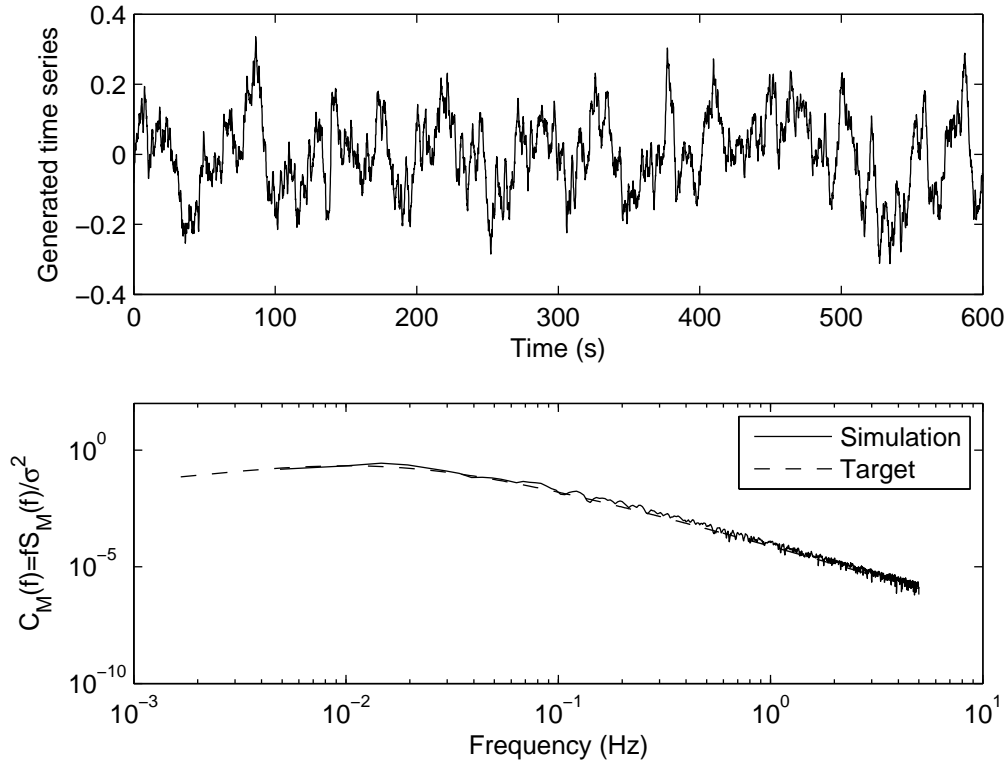


Figure 4.3: Time series of along-wind base bending moment

4.4 Dynamic analysis and results

By applying a static-wind load calculated using the methods presented above, a static deflection can be calculated. Figure 4.5 shows EWSL in both along- and across-wind direction.

By applying the static load to the structure and calculating the deflection, Ritz-vectors was defined. By reducing the system and once again solving the eigenvalue problem, the fundamental frequency is determined to 0.1574 Hz in both directions. Table 4.1 shows the difference between the first eigen frequency in the along- and across-wind direction for the two systems.

Table 4.1: First eigen frequency in the along- and across-wind direction for the full and reduced system.

	Frequency along, Hz	Frequency across, Hz
Full system	0.1574	0.1574
Reduced system	0.1574	0.1574
Difference	0.0%	0.0%

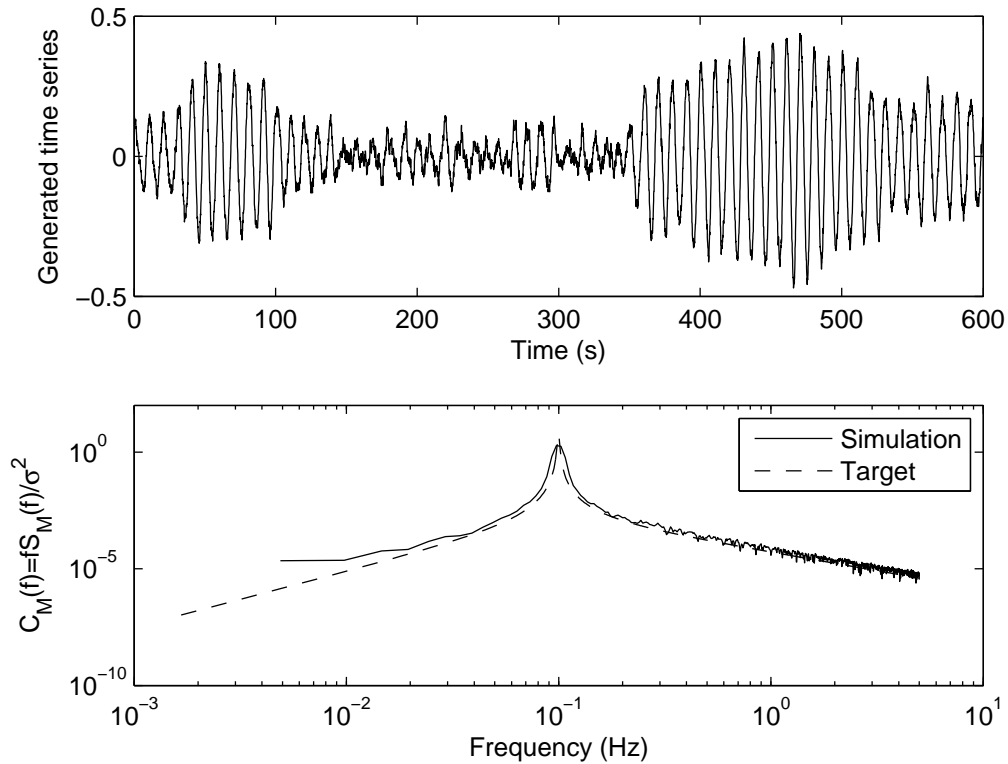


Figure 4.4: Time series of across-wind base bending moment

With similar frequencies in the full and reduced systems the Ritz-vector are sufficiently accurate and can be used in further dynamic simulation, given the proximity of the natural frequencies in the full and reduced system. Important to notice is that the original system consisting of 8160 dofs has now been reduced to a system with only two dofs.

During a 600 second long time-series simulation, the acceleration levels in a point at the top of the building was recorded, both in the along- and across-wind direction. The simulation time for the whole system was 3690 seconds. After the system had been reduced the simulation time was reduced to 0.23 seconds. Figures 4.6 and 4.7 show the acceleration response of the full and reduced system in both along- and across-wind direction.

Table 4.2: Time to complete simulation of a 600 second long wind-load.

	Time, s
Full system	3690
Reduced system	0.23

Furthermore the RMS value of the acceleration can be calculated to show the similarity between the two systems. Table 4.3 shows the difference in RMS value.

Table 4.3: RMS value for accelerations at the top of the buildings in along- and across-wind direction.

	RMS along	RMS across
Full system	0.5590	0.1092
Reduced system	0.5570	0.1099
Difference	0.52%	-0.60%

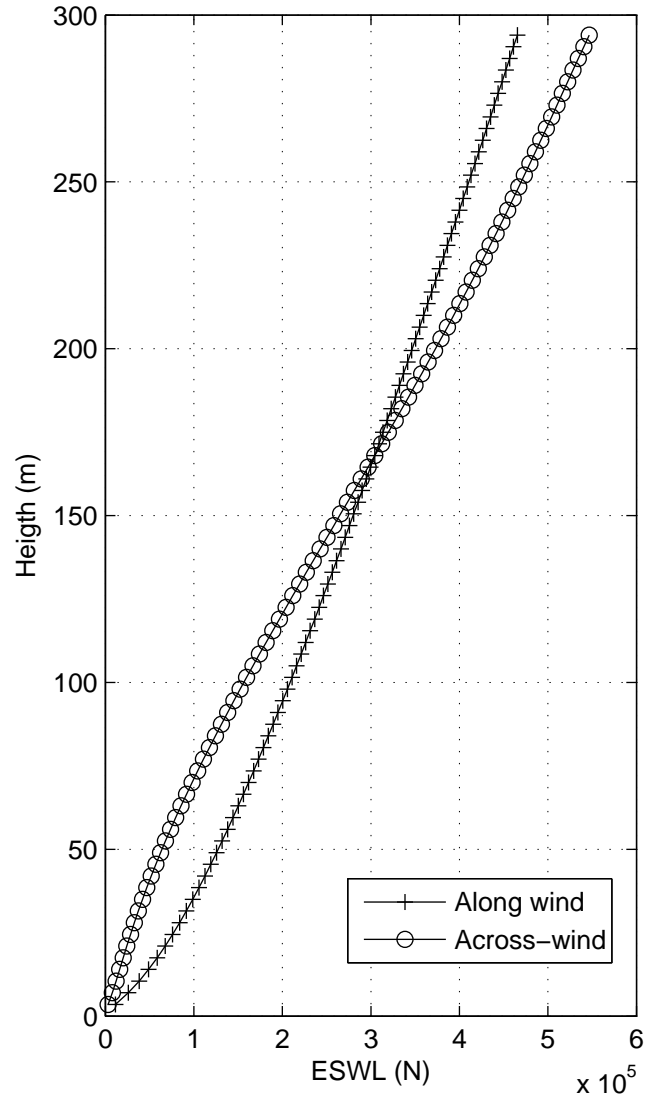


Figure 4.5: Equivalent static wind-load applied on each floor

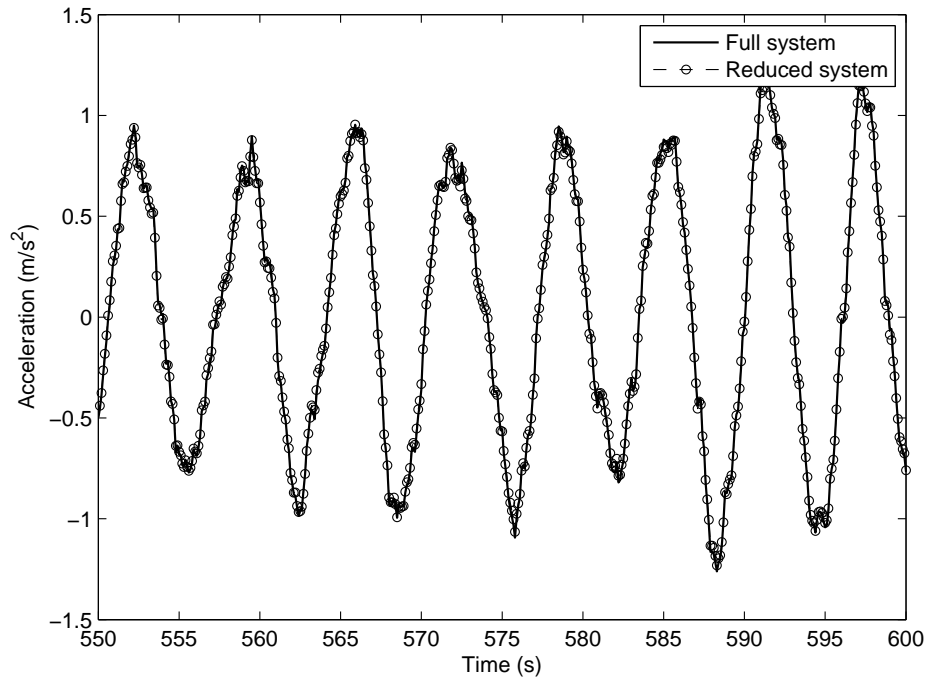


Figure 4.6: Comparison between the full and reduced system in the along-wind direction

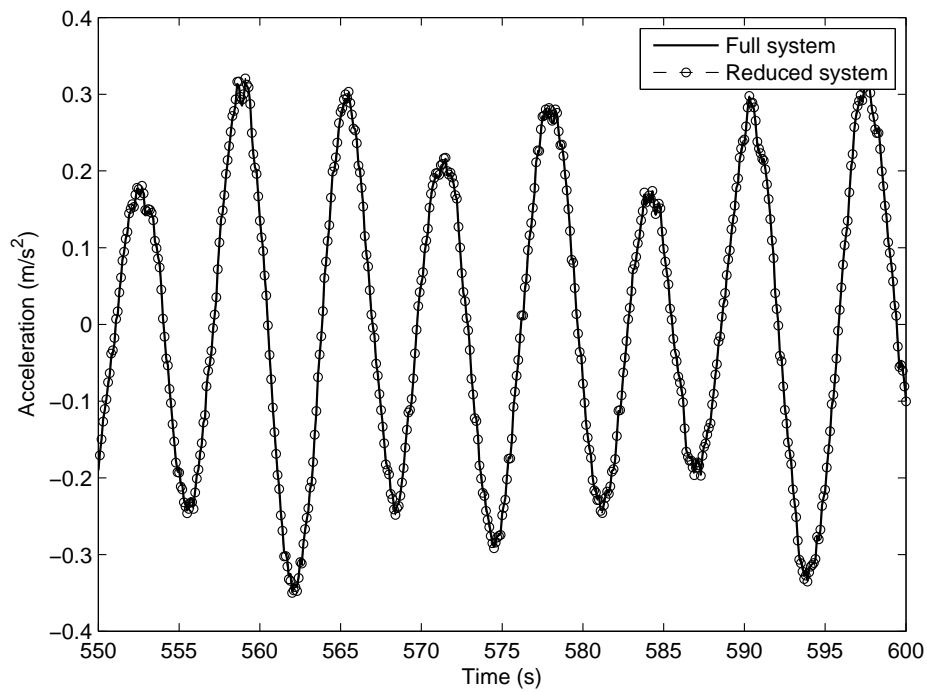


Figure 4.7: Comparison between the full and reduced system in the across-wind direction

5. Vibration-reduction measures

There are several ways to reduce the vibrations occurring in tall buildings from wind. Some of these are discussed in following sections.

A building's damping is a measure of its ability to dissipate energy. Some energy is dissipated within the building material itself, while some dissipates due to friction between structural elements. With taller and slender building, the structural damping may not be sufficient to prevent a building from oscillating in a manner which causes discomfort for the occupants. Due to this, various sort of auxiliary damping has to be introduced to keep acceleration at an acceptable level.

Dampers can be either active, passive or hybrids. Passive dampers usually operate through either a material based dissipation system or through the generation of a counteracting inertia force. The material based dampers can use many properties to increase damping, such as viscous, elastic-viscous, hysteretic, friction and electromagnetic properties. Creating a counteracting force involves adding a mass to the structural system, either solid or liquid. While many different active dampers are available, active mass dampers (AMD) and active variable stiffness devices (AVSD) are the most common. Passive dampers are often tuned to the specific structure and operate within a limited range of loading conditions, while active dampers cover a wider range. Active dampers on the other hand are more expensive and require more maintenance [34].

The sections below aim at giving the reader an overview of different vibration reduction measures.

5.1 Structural methods

Many factors make up a building's structural damping. These include structural material, soil and foundation conditions, architectural finish, joints, and non-structural members. Since there is no theoretical way to estimate the damping of a building, estimations are based on full-scale data, resulting in a significant scatter.

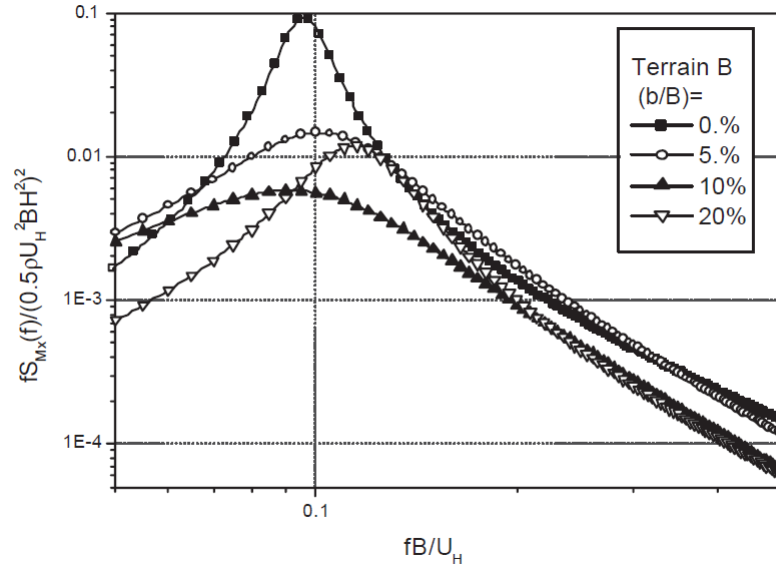


Figure 5.1: Effect of beveled corners on the BBM [30].

Table 5.1 shows a summary of different energy dissipation mechanics in buildings [32].

Table 5.1: Damping mechanics [32].

	Energy dissipation inside			Energy dissipation outside		
	Solid	Liquid	Gas	S-S	S-L	S-G
Friction	Internal friction damping	-	-	External friction damping	-	-
Viscosity	-	Internal viscous damping		-	External viscous damping	
Radiation	-			Radiation damping		-
Interaction	-			-	Hydrodynamic damping	Aerodynamic damping
Plasticity	Hysteretic damping	-		-		

One way to reduce acceleration levels is to change the shape of the structure. For instance, adding bevels or concave corners significantly reduces the peak around the reduced frequency of 0.1 Hz, thus resulting in a lower energy at frequencies close to the fundamental frequency of the building. Figures 5.1 and 5.2 show the reduction cause by different corner modifications. Another way is to make sure that the vortex phenomenon does not occur over several stories of a building, for example by using setbacks and other various geometries along the building height.

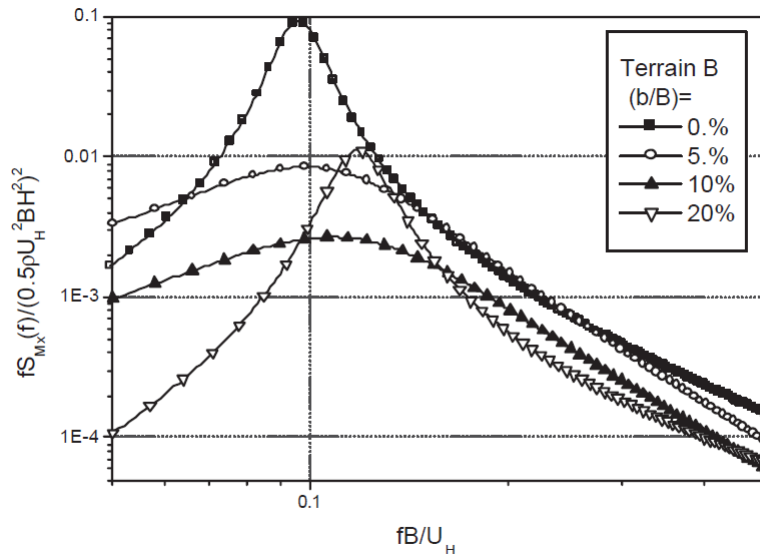


Figure 5.2: Effect of concave corners on the BBM [30].

5.2 Passive methods

Viscoelastic dampers

As the name suggest, viscoelastic dampers use materials with viscoelastic properties. Completely viscous materials resist strain linearly with respect to the velocity of the loading when a external load is applied with time, while completely elastic materials return to their original state once the external load is removed. A viscoelastic materials combine these two properties. Viscoelastic dampers work by transferring mechanical energy into heat in the material [23]. Different kinds of viscoelastic dampers are available [35]. The first one is by simply applying a viscoelastic material to a vibrating structural member. A second type is achieved by applying a constraint layer above the viscoelastic layer. This causes the material to not only dissipate energy through extensional deformation, but also through shear. The final and most typical configuration is done by alternating layers of structural parts and viscoelastic materials. Figure 5.3 shows a schematic view of the three usages. The properties of the material can vary with environmental temperature and excitation frequency. One way of determining the properties of a typical VE-damper is by applying a periodic displacement and plotting it and the corresponding shear stress. This gives a hysteresis loop, where the area of the loop represents the energy loss [35].

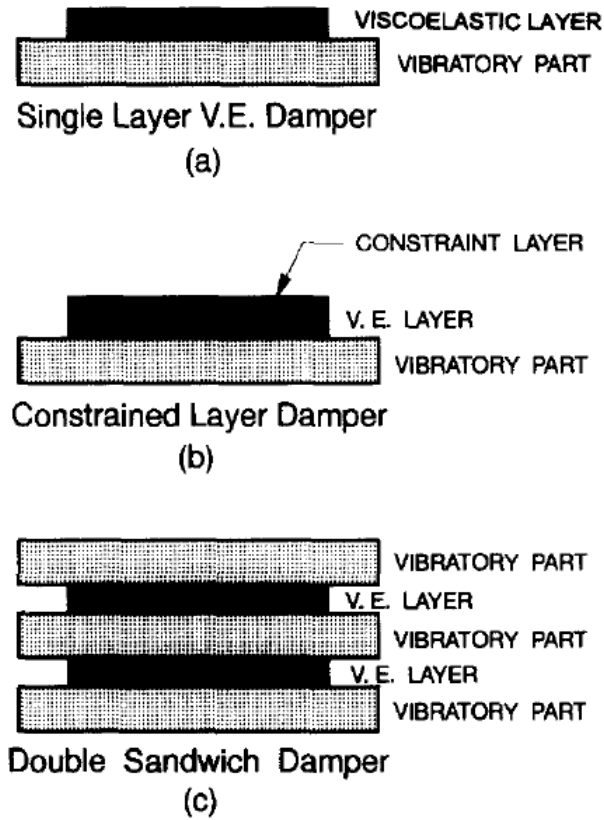


Figure 5.3: Different usage of visco-elastic material [35]

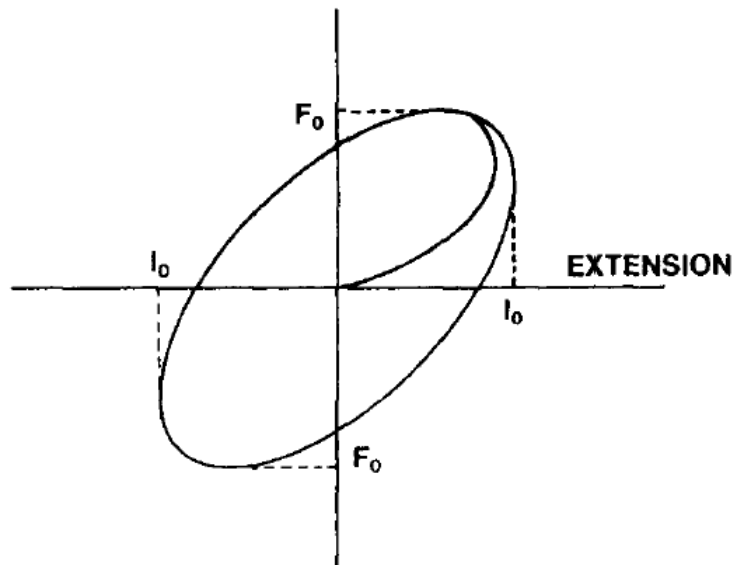


Figure 5.4: Typical hysteresis-loop [35]

The original World Trade Center buildings were the first major buildings that used viscoelastic dampers to inhibit excessive acceleration. Approximately 10 000 dampers were installed in each of the towers [23]. Since then, the development have progressed and in a more modern example, the Columbia SeaFirst building in Seattle use a mere 280 dampers to reduce acceleration in the 286 m building [35]

Viscous dampers

Unlike visco-elastic dampers, completely viscous dampers require some form of housing for the viscous fluid. Figure 5.5 shows a typical viscous damper. A piston moves trough chamber filled with liquid. The liquid pushes through orifices around and through the piston head. On the upstream side of the piston head, the fluid velocity is very high and a majority of it converts into kinetic energy. Once it passed the piston head it slows down and the kinetic energy is lost into turbulence. The pressure difference on each side of the piston head produce a force which resists the motion of the damper [36]. Some buildings that use viscous damper include Tianjin International Trade Center (250 m), Silvertie Center (265 m) and Tianjin FULI building (403 m) [37].

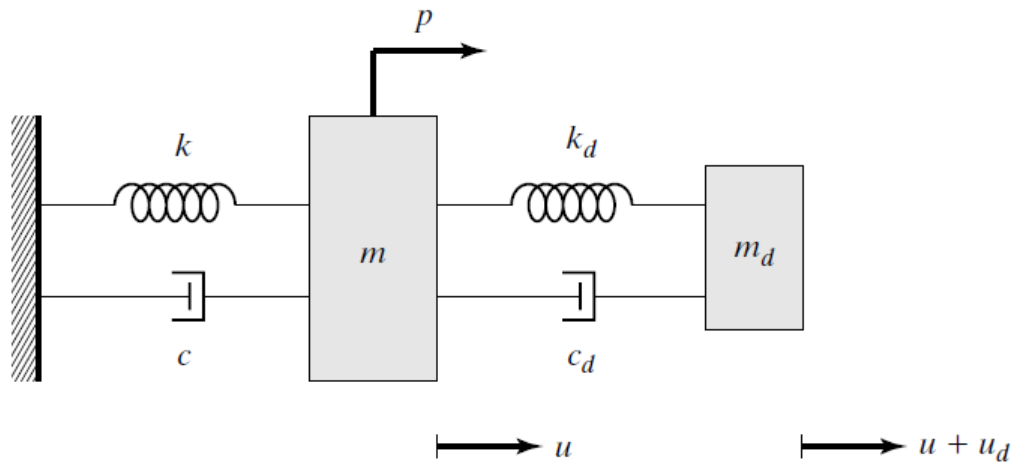


Figure 5.6: SDOF-system with a tuned mass damper [38].

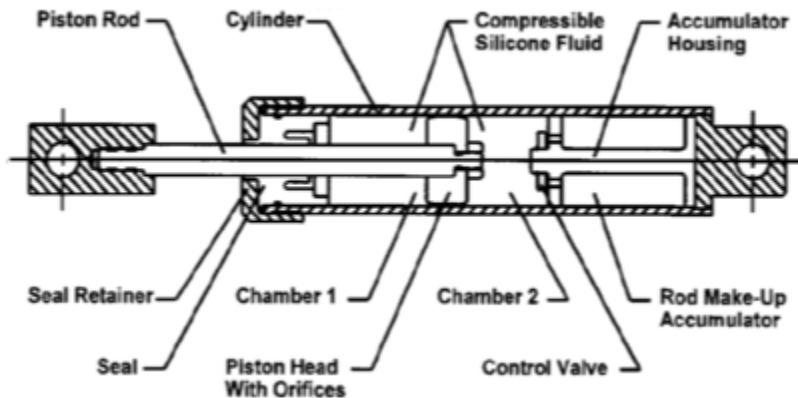


Figure 5.5: Typical viscous damper [36]

Tuned Mass Dampers

A common way of adding damping to a building is the use of a tuned mass damper. A secondary mass is attached to the structural system using springs and dampers. Figure 5.6 shows a SDOF-system with a tuned mass damper.

Figure 5.7 shows the principal design of a tuned mass damper installed in buildings such as John Hancock Tower, Citicorp Center, Canadian National Tower and Chiba Port Tower [38]. Early use of tuned mass dampers involved complex bearing and damper mechanics, were very spacious and quite expensive. By combining tuned mass dampers with visco-elastic dampers discussed in previous chapter a more efficient way

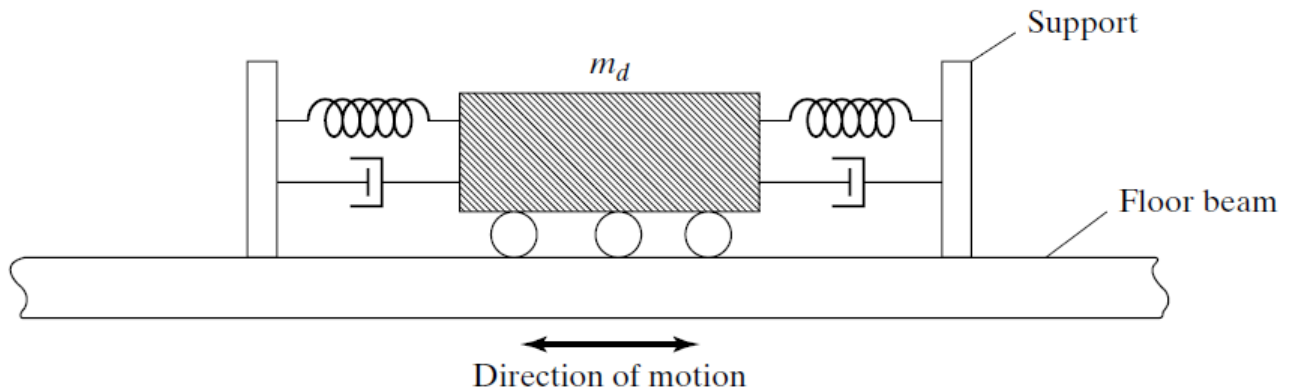


Figure 5.7: Principal design for translational tuned mass damper [38].

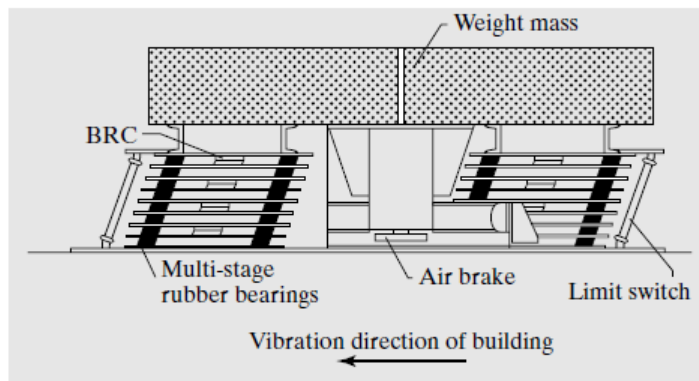


Figure 5.8: Tuned mass damper on visco-elastic dampers [38].

of damping structures has been developed. Figure 5.8 shows the principal layout.

Another way of overcoming the problem with complex bearing and mechanical solution is to support the mass with cables, thus creating a pendulum. The most famous is the pendulum tuned mass damper in Taipei 101, a 660 tons mass with a diameter of 5.5 meters, it hangs between the 92nd and 87th floor. Though a theoretical simple solution one limitation is that the fundamental frequency of the system is dependent on the pendulum length, which for slow periods may become larger than a typical floor height.

Tuned liquid dampers

Tuned liquid dampers are practically the same as tuned mass dampers, but the solid mass has been replaced by a body of liquid. The energy dissipation occurs from mech-

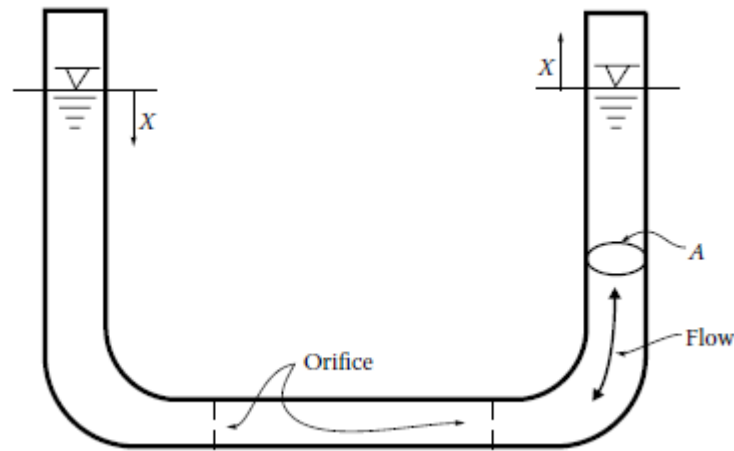


Figure 5.9: Basic liquid column damper [23].

anism such as viscous boundary layers, turbulence in the liquid and wave breaking. Liquid dampers can be divided into two categories, tuned sloshing dampers (TSD) and tuned liquid column dampers (TLCD) [23].

Sloshing dampers fall roughly within one of two categories, shallow- or deep-water dampers. Shallow-water dampers primarily dissipates energy through internal fluid viscous forces and wave breaking. The damping can be further enhanced by adding plastic beads or a lip along the surface parameter. In deep-water dampers, the addition of baffles or screens can further increase the damping of the system [39].

Considering their simplicity, low maintenance and cheap cost, TSD dampers are a valid options for many types of building. It also has the advantage of allowing incorporation into other building systems, such as sprinklers [23].

As with the sloshing damper, liquid column dampers work through the displacement of liquid. While the workings of sloshing dampers are complicated, the theory for column dampers is more simple and accurate. The technique was originally developed to reducing pitching motion in ships due to wave motion [40]. In recent years it has become a valid option for reducing motion in buildings, with easy application in both new buildings or for retrofitting in older ones. The TLCD consists of rigid piping with a liquid in it, and dissipate energy through internal viscous forces. The amount of damping can be adjusted by adding orifices in the piping system. A schematic view is shown in Figure 5.9. Unlike sloshing dampers, column dampers does not add any significant mass to the structure.

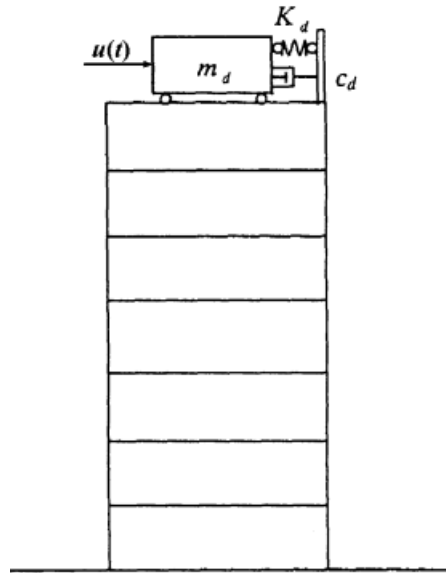


Figure 5.10: Schematic view of an active tuned mass damper [41].

5.3 Active methods

Active tuned mass dampers

A common way of gaining more efficiency out of a tuned mass damper is by adding an active control system. By adding a small control force to the mass, the building's response can be dramatically reduced [41]. Since an external force determines the damping, a smaller mass can be used, which makes retrofitting easier. Adding an active system also allows the tuned mass damper to operate within a frequency range instead of being tuned to one specific frequency [42]. Figure 5.10 shows a schematic view of a active tuned mass damper.

Active variable stiffness devices

Active variable stiffness devices consist of additional bracing along a building's structural system. These braces are attached to locking devices which can lock or unlock on certain floors when a building is subjected to external forces. Since the dynamics of locking and unlocking the bracing system is non-linear, different control theories have to be used compared to active tuned mass dampers. One theory suggests activating the locking devices so that the building's frequency shifts as far away from the external force's frequency as possible. Another theory is locking the system when the displacement and velocity act in the same direction, while unlocking the system if they act

opposite each other [43]. Furthermore the locking devices can be activated by a small amount of energy and since the devices does not induce any vibrations of its own, the control system does not have to perform as accurately as with active tuned mass dampers [44].

6. Conclusion and discussion

Structural designers and building owners should be aware of the complexity associated with wind protection engineering. Not only are there uncertainties in the approximation of the dynamic response itself, but since people react so differently to the phenomenon one has to take extra consideration when evaluating acceptable accelerations in a building. Careful consideration has to be taken regarding the building's properties such as natural frequency and stiffness, type of storms likely to occur at its location and whether it is to be an office building, residential or mixed. Since removing all sorts of noticeable vibrations is uneconomical from a structural point of view, owners have to decide how high vibration levels can be tolerated without affecting the rental or sale plans. Too much vibrations and contracts might be cancelled and the reputation of the building and company damaged, while reducing vibrations too much will result in high building costs.

While the Eurocode does not provide any formulas for accelerations in buildings over 200 meters, some minor modifications of the formulas can provide designers with an estimation of the response in an early design phase. Designers should be aware that this is only a rough estimate, due to the complexity involving wind loads. When dealing with tall and slender buildings, wind-tunnel testing is often recommended to gain more insight into a building's dynamic behaviour. With the ever growing skyline, estimating acceleration becomes more difficult due to interference with surrounding buildings.

Numerical simulation of a system reduced with Ritz-vectors showed a good correlation with the full system, while saving substantial computational time. However, one should be aware that with even taller and more slender buildings than the idealised one used here, higher modes become more influential and neglecting them may result in an underestimation of the actual response.

With even higher and taller buildings than the one used for this thesis, higher modes contribute to a dynamic response as well. To estimate the second mode shape, using the equivalent static wind load is not enough, other methods need to be used. One method could be trying different wind-speeds when calculating the EWSL, since certain wind-speeds will cause vortex shedding on a few levels of a building, and thus a greater static load.

A. Appendix

A.1 Appendix A

```
1
2 b=25;           %Building breadth
3 w=25;           %Building width
4 n=85;           %Number of floors
5 deltaH=3.5;    %Floor height
6
7 %Empty coordination matrices.
8 LillaCord=zeros(16,2);
9 Coord=zeros(16*n,2);
10
11
12 %Coordination matrix for one floor.
13 for k=1:4
14     LillaCoord((4*k-3):(4*k),1)=0:(2*b)/3:2*b;
15     LillaCoord((4*k-3):(4*k),2)=(2*b)/3*(k-1);
16 end
17
18 %Floor matrix assembled for the full structure.
19 for l=1:n
20     Coord((16*l-15):16*l,3)=deltaH*(l-1);
21     Coord((16*l-15):16*l,1:2)=LillaCoord;
22 end
23
24 %Empty dof matrix created.
25 Dof=zeros(length(Coord),6);
26
27 for k=1:length(Coord)
28     Dof(k,1:6)=(6*(k-1))+(1:6);
29 end
30
31 %Empty Edof matrix for one flooer created.
32 LillaEdof=zeros(40,13);
33
34 %DOFs in each node generated.
```

```

35 for k=1:16
36     LillaEdof(k,:)=[k 6*(k-1)+(1:6) 6*(k-1)+96+(1:6)];
37 end
38
39 for k=1:4
40     LillaEdof(3*k+(14:16),1)=3*k+(14:16)';
41     LillaEdof(3*k+(14:16),2:13)=[24*(k-1)+(97:108); ...
42         24*(k-1)+(103:114); 24*(k-1)+(109:120)];
42 end
43
44 for k=1:4
45     LillaEdof(3*k+(26:28),1)=3*k+(26:28)';
46     LillaEdof(3*k+(26:28),2:13)=[6*(k-1)+(97:102) ...
47         6*(k-1)+(121:126); 6*(k-1)+(121:126) 6*(k-1)+(145:150); ...
48         6*(k-1)+(145:150) 6*(k-1)+(169:174)];
47 end
48
49 %Edof matrix assembles for the full structure.
50 for k=1:(n-1)
51     Edof((40*k-39):40*k,:)=[40*(k-1)+LillaEdof(:,1) ...
52         96*(k-1)+LillaEdof(:,2:13)];
52 end
53
54 %Coordinated for each node extracted.
55 [ex,ey,ez]=coordxtr(Edof,Coord,Dof,2);
56
57 %The structure is plotted.
58 eldraw3(ex,ey,ez)
59 text(Coord(:,1),Coord(:,2),Coord(:,3),num2str(Dof(:,1:2)))
60
61 %Material parameters.
62 E=210e9;
63 A=0.3;
64 Iy=0.015;
65 Iz=0.015;
66 K=0.5;
67 G=80e9;
68
69 ep=[E G A Iy Iz K];
70
71 % Total number of dofs.
72 s=max(max(Edof));
73
74 %Empty stiffness, mass and damping matrices created..
75 K=zeros(s);
76 M=zeros(s,1);
77 C=zeros(s);
78
79 %Orientation of structural members, local z axis parallel to the ...
80     global z.
81 %axis

```

```

81 eo=[0 1 0];
82 eo2=[0 0 1];
83 eo3=[0 0 1];
84
85 %Assembly of stiffness matrix.
86 tic
87 for i=1:40:40*(n-1)
88     for j=0:15
89         Ke=beam3e(ex(i+j,:),ey(i+j,:),ez(i+j,:),eo,ep);
90         K=assem(Edof(i+j,:),K,Ke);
91     end
92 end
93 toc
94 tic
95 for i=17:40:40*(n-1)
96     for j=0:11
97         Ke=beam3e(ex(i+j,:),ey(i+j,:),ez(i+j,:),eo2,ep);
98         K=assem(Edof(i+j,:),K,Ke);
99     end
100 end
101 toc
102 tic
103 for i=29:40:40*(n-1)
104     for j=0:11
105         Ke=beam3e(ex(i+j,:),ey(i+j,:),ez(i+j,:),eo3,ep);
106         K=assem(Edof(i+j,:),K,Ke);
107     end
108 end
109 toc
110
111 %Assembly of mass matrix.
112 for k=1:6:s
113     M(k:(k+2))=1;
114 end
115
116 for k=4:6:s
117     M(k:(k+2))=0.001;
118 end
119
120 M=0.32e5*diag(M);
121
122 %Boundry conditions, cantilever beams at the first floor.
123 bc1=1:96;
124
125 %Rayleigh damping created from mass and stiffness matrix and the ...
    two lowest
126 %eigen-frequencies.
127 a0=0.01*2*0.9889*3.0668/(0.9889*3.0668)
128 a1=0.01*2/(0.9889*3.0668)
129 C=a0*M+a1*K;
130

```

```

131 %Mass and stiffness matrices reduced.
132 Ksparse=sparse(K(97:end,97:end));
133 Msparse=sparse(M(97:end,97:end));
134
135 %Mass and stiffness matrices with members at first floor removed
136 Kfull=(K(97:end,97:end));
137 Mfull=(M(97:end,97:end));
138
139 %The seven lowest eigen-frequencies are calculated
140 [Xsparse,Lsparse]=eigs(Ksparse,Msparse,7,'sm');
141
142 %A subroutine created the equivalent static wind load on each ...
    floor for two
143 %directions.
144 [Ptot,p]=Modell(n-1,deltaH,w);
145
146 %Empty force matrices.
147 q=zeros(s,1);
148 q2=zeros(s,1);
149
150 %Generated ESWL applied in respective dof on each floor
151 for k=1:4
152 q(Edof((4*k)-3):40:end,8)=Ptot/4;
153 end
154
155 for k=1:4
156 q2(Edof(k:40:end,9))=p/4;
157 end
158
159 % Boundry condiction
160 bc2=[bc1' zeros(length(bc1),1)];
161
162 %The static displacement for each dof is solved
163 a=solveq(K,q,bc2);
164 a2=solveq(K,q2,bc2);
165
166 %Displacements are extracted and plotted
167 Ed=extract(Edof,a);
168 Ed2=extract(Edof,a2);
169
170 figure()
171 eldraw3(ex,ey,ez,[2 1 0])
172 [magnfac]=eldisp3(ex,ey,ez,Ed);
173 eldisp3(ex,ey,ez,Ed(:,:),[1 1 0],magnfac*5)
174 axis([-5 65 -5 65 0 (n*deltaH+10)])
175
176 figure()
177 eldraw3(ex,ey,ez,[2 1 0])
178 [magnfac]=eldisp3(ex,ey,ez,Ed2);
179 eldisp3(ex,ey,ez,Ed2(:,:),[1 1 0],magnfac*5)
180 axis([-5 65 -5 65 0 (n*deltaH+10)])

```

```

181
182 %Reduction of full matrixes using the static deflection
183 KritzFull=[a a2]'*K*[a a2];
184 MritzFull=[a a2]'*M*[a a2];
185 CritzFull=[a a2]'*C*[a a2];
186
187 %Solving the eigenvalue-problem for the reduced system
188 [XritzFull,LritzFull]=eigen(KritzFull,MritzFull);
189
190 %A subroutine generates a time-series of a wind-load in two ...
    directions
191 [yFullAcross,yFullAlong]=TimeSeries();
192
193 %Empty initial displacement and velocity vectors are created.
194 d0=zeros(s,1);
195 v0=zeros(s,1);
196
197 %Empty force matrix created
198 f=zeros(s,length(yFullAlong));
199
200 %The generated wind-force is applied its respective dofs on each ...
    floor.
201 for k=1:4
202 f(Edof(((4*k)-3):40:end,8),:)=flipud(yFullAlong)/4;
203 end
204
205 for k=1:4
206 f(Edof(k:40:end,9),:)=flipud(yFullAcross)/4;
207 end
208
209 %Parameters for time-stepping, Full system
210 dt=0.1; %Time-step
211 tottime=600; %Total time
212 time=[0:dt:totime]; %Time intervall
213 dof=[s-5 s-4]; %DOFs where accelerations are stored
214 alpha=0.25; %Average acceleration (trapezoidal) rule
215 delta=0.5; %Average acceleration (trapezoidal) rule
216 nsnap=max(size(time));
217 nhist=1;
218
219 ip=[dt tottime alpha delta [nsnap nhist time dof]];
220 pdisp=bc2;
221
222 %Time-stepping performed
223 tic
224 [Dsnap,D,V,A]=step2(K,C,M,d0,v0,ip,f,pdisp);
225 wholeSys=toc
226
227
228 %Parameters for time-stepping, Reduced system
229 dt=0.1; %Time-step

```

```

230 tottime=600;           %Total time
231 time=[0:dt:tottime]; %Time intervall
232 dof=[1 2];           %DOFs where accelerations are stored
233 alpha=0.25;         %Average acceleration (trapezoidal) rule
234 delta=0.5;          %Average acceleration (trapezoidal) rule
235 nsnap=max(size(time));
236 nhist=1;
237
238 %Empty initial displacement and velocity vectors are created.
239 d0ritz=zeros(2,1);
240 v0ritz=zeros(2,1);
241
242 ip=[dt tottime alpha delta [nsnap nhist time dof]];
243 pdisp=[];
244
245 %Forces reduced using Ritz-vectors
246 fritz=[a a2]*f;
247
248 %Time-stepping performed
249 tic
250 [DsnapRitz,Dritz,Vritz,Aritz]=step2(KritzFull,CritzFull,MritzFull,d0ritz
251 ,v0ritz,ip,fritz,pdisp);
252 ritzSys=toc
253
254 %Accelerations converted from redcued system to full system.
255 Afull=[a a2]*Aritz;
256
257 %Accelerations at the top of the buildings plotted
258 figure();
259 plot(time,A(1,:), 'k', 'LineWidth',1.0);hold on
260 plot(time,Afull(8155,:), 'k--o', 'MarkerSize',4);
261 legend('Full system','Reduced system')
262 ylabel('Acceleration (m/s^2)')
263 xlabel('Time (s)')
264 set(gca, 'LooseInset', get(gca, 'TightInset'))
265
266 figure();
267 plot(time,A(2,:), 'k', 'LineWidth',1.0);hold on
268 plot(time,Afull(8156,:), 'k--o', 'MarkerSize',4);
269 legend('Full system','Reduced system')
270 ylabel('Acceleration (m/s^2)')
271 xlabel('Time (s)')
272 set(gca, 'LooseInset', get(gca, 'TightInset'))
273
274 %Root mean square of the accelerations calculated
275 rmsAlongWhole=rms(A(1,:))
276 rmsAlongRitz=rms(Afull(8155,:))
277
278 rmsAcrossWhole=rms(A(2,:))
279 rmsAcrossRitz=rms(Afull(8156,:))

```

A.2 Appendix B

```

1 function [yFullAcross,yFullAlong]=TimeSeries();
2 %
3 %%%%%%%%%%%%%%%%%%%%%%%%%%%%%%%%%%%%%%%%%%%%%%%%%%%%%%%%%%%%%%%%%%%%%%%%%
4 %This simulates Gaussian process given the Power Spectrum Density
5
6
7 dt = 0.1; % sampling interval
8 N = 6000; % number of time instances
9 T = dt*N; % length of time series to be simulated
10 time = (0:dt:T)'; % time vector
11 ntp = length(time);
12
13 RMS=0.5*1.22*30^2*50*300^2
14 %%%%%%%%%%%%%%%%%%%%%%%%%%%%%%%%%%%%%%%%%%%%%%%%%%%%%%%%%%%%%%%%%%%%%%%%%
15 % delta_f = 1/T; % Sampling frequency (Hz)
16 f = (1/T:1/T:ntp/2/T)'; % frequency vector
17 nfp = length(f);
18
19 fp=0.09864;
20 sp=0.1606;
21 beta=0.01154;
22 alpha=2.671;
23
24 for k=1:length(f)
25
26 PSD(k)=(RMS^2*sp*beta*(f(k)/fp)^alpha)/((1-(f(k)/fp)^2)^2
27 +beta*(f(k)/fp)^2*(0.151^2));
28 %
29 %
30 %
31
32 end
33 % *(0.5*1.22*32^2*30*90^2)^2/f(k)
34 amp = sqrt(PSD)'; % sqrt of PSD = amplitude spectrum
35 phase = 2*pi*rand(nfp,1); % random phase
36 Y = amp.*exp(sqrt(-1)*phase); % complex noise
37 Y = [Y; flipud(conj(Y))]; % Replicate complex conj
38 Y = [0;Y]; % Give it zero mean
39 %The generated time series
40 scale =200; % scaling factor
41 y = scale*ifft(Y,ntp); % Inverse transform
42 %%%%%%%%%%%%%%%%%%%%%%%%%%%%%%%%%%%%%%%%%%%%%%%%%%%%%%%%%%%%%%%%%%%%%%%%%
43 %Power Spectral Density Verification
44 [Pxx,f1] = pwelch(y,[],[],[],1/dt);
45 target = PSD;
46 figure();
47 subplot(2,1,1); plot(time,y,'k'); xlabel('Time (s)');

```

```

48 ylabel('Generated time series')
49 subplot(2,1,2); loglog(f1,Pxx,'k')
50 hold on
51 loglog(f,target,'--k'); xlim([0.001 10]);ylim([1e-10 100]);
52 xlabel('Frequency (Hz)');ylabel('C_M(f)=fS_M(f)/\sigma^2');
53 legend('Simulation','Target')
54 area_exact = trapz(f,target); display(area_exact);
55 area_simulated = trapz(f1,Pxx); display(area_simulated);
56 % should be equal to area_exact
57 var_simulated = var(y); display(var_simulated);
58 % should be equal to area_simulated
59
60 % -----
61
62
63 U_h=30;
64 H=297.5;
65 B=50;
66 % L_h=1200;
67 I_h=0.29;
68 alpha=0.27;
69 Lz=100*sqrt(H/30);
70 cg=2*I_h*(0.49-0.14*alpha)/(1+(0.63*(sqrt(B/H)/Lz)^0.56)/((H/B)^0.07));
71 for k=1:length(f)
72 sd(k)=0.9./(sqrt(1+6*(f(k)*H/U_h)^2)*(1+3*f(k)*B/(U_h)));
73 f2(k)=4*f(k)*Lz/U_h/(1+71*(f(k)*Lz/U_h)^2)^(5/6);
74 r(k)=1/(1+20*f(k)*B/U_h);
75 FD(k)=RMS^2*I_h^2*f2(k)*sd(k)*(0.57-0.35*alpha+
76 2*r(k)*sqrt(0.053-0.042*alpha))/(cg^2*f2(k));
77 end
78 %
79 %
80 %
81
82 % *(0.151*0.5*1.22*32^2*30*90^2)^2/f(k)
83 FD=FD';
84 amp2 = sqrt(FD); % sqrt of PSD = amplitude spectrum
85 phase = 2*pi*rand(nfp,1); % random phase
86 Y = amp2.*exp(sqrt(-1)*phase); % complex noise
87 Y = [Y; flipud(conj(Y))]; % Replicate complex conj
88 Y = [0;Y]; % Give it zero mean
89 %The generated time series
90 scale2 =200; % scaling factor
91 y2 = scale2*ifft(Y,ntp); % Inverse transform
92 %%%%%%%%%%%%%%%%%%%%%%%%%%%%%%%%%%%%%%%%%%%%%%%%%%%%%%%%%%%
93 %Power Spectral Density Verification
94 [Pxx2,f2] = pwelch(y2,[],[],[],1/dt);
95 target2 = FD;
96 figure();
97 subplot(2,1,1); plot(time,y2,'k'); xlabel('Time (s)');
98 ylabel('Generated time series')

```

```

99 subplot(2,1,2); loglog(f2,Pxx2,'k')
100 hold on
101 loglog(f,target2,'--k'); xlim([0.001 10]);ylim([1e-10 100]);
102 xlabel('Frequency (Hz)');ylabel('C_M(f)=fS_M(f)/\sigma^2');
103 legend('Simulation','Target')
104 area_exact = trapz(f,target); display(area_exact);
105 area_simulated = trapz(f2,Pxx2); display(area_simulated);
106 % should be equal to area_exact
107 var_simulated = var(y2); display(var_simulated);
108 % should be equal to area_simulated
109 %
110 % figure()
111 % loglog(f2,Pxx2,f,target2,'r',f1,Pxx,f,target,'r')
112
113
114
115 ff=linspace(1,0,84)';
116
117 yFullAcross=ff*y'/(84*3.5*ff'*ff);
118 yFullAlong=ff*y2'/(84*3.5*ff'*ff);
119 end

```

A.3 Appendix C

```

1 function [Ptot,p]=modell(i1,i2,i3)
2
3 n=i1; %Number of floors
4 L=i2; %Floor height
5 %Empty coordinate matrices
6 ex=zeros(n,2);
7 ey=zeros(n,2);
8 ez=zeros(n,2);
9 H=L*n; %Building height
10 eo=[0 1 0]; %Local coordinates in realation ...
    to the
11 %global
12
13 % Wind parameters
14 Ubasic=30; %Reference speed at 10 meters.
15 cd=1.3; %Drag coefficient
16 w=50; %Building width
17 rho=1.22; %Air density
18 f0x=0.1574; %First along-wind freq.
19 f0y=0.1574; %First across-wind freq.
20 T=600; %Observation time
21 damping=0.01; %Structural damping
22
23 %Terrain coefficient
24 z0=1;

```

```

25 u=0.094;
26
27 % Floorheights saved in vector
28 x=L:L:H;
29 % Average wind-speed per floor
30 mean_speed=u/0.4*log(x./z0)*Ubasic;
31 % Roughness factor
32 alpha=0.3;
33
34
35 % -----Along-wind loads
36
37 % Average wind-load per floor
38 Pmean=zeros(length(x),1);
39     for j=1:length(x)
40
41         Pmean(j)=0.5*rho*(mean_speed(j))^2*cd*L*w;
42
43     end
44
45 % Base bending moment calculated from average floor load.
46 Mmean=0
47     for j=1:length(x)
48
49         Mmean=Mmean+Pmean(j)*x(j);
50
51     end
52
53 % Background factor
54 Tlength=100*(0.6*H/30)^0.5;
55 B=1/(1+3/2*sqrt((w/Tlength)^2 + (H/Tlength)^2 + (w*H/(Tlength^2)))));
56 gb=sqrt(2*log(f0x*T))+0.6/sqrt((2*log(f0x*T)));
57 Ih=1/log(0.6*H/z0);
58 G_mb=2*gb*Ih*sqrt(B);
59
60
61 % Resonant factor
62 phiY=11.5*w*f0x/(mean_speed(round(0.6*length(mean_speed))));
63 phiZ=11.5*H*f0y/(mean_speed(round(0.6*length(mean_speed))));
64 Gy=1/2;
65 Gz=3/8;
66 S=1/(1+sqrt((Gy*phiY)^2 + (Gz*phiZ)^2 + ...
67     (2*Gy*phiY*Gz*phiZ/pi())^2));
68 N=f0x*Tlength/(mean_speed(round(0.6*length(mean_speed))));
69 E=4*N/((1+71.8*N^2)^(5/6));
70 gr=gb;
71 G_mr=2*gr*Ih*sqrt(S*E/damping);
72
73 Mr=Mmean*G_mr;
74 %Reference mass

```

```

75 m=2.88e5
76
77 %Empty force vectors
78 Pr=zeros(length(x),1);
79 Pb=zeros(length(x),1);
80 bot=0;
81
82 %Forloop creating the EWSL
83 for j=1:length(x)
84
85     top=m*L*(x(j)/H);
86     bot=m*H^3/(3*H);
87     Pr(j)=top*Mr/bot;
88
89     Pb(j)=G_mb*Pmean(j);
90
91 end
92 Ptot=(Pb+Pr);
93 % -----Across-wind load
94 % Generalized mass, constant mass
95 m0=2.88e5
96 Mi=m0*H^3/(3*H^2);
97
98 % The exponents of the mean wind profiles for the terrain
99 % categories A, B, C and D are 0.12, 0.16, 0.22 and 0.30,
100 % and the corresponding
101 % gradient heights are 300, 350, 400 and 450 m,
102 % Across wind-base moment coeffiecient
103 a_db=1;
104 a_w=4;
105 a_hr=H/w;
106
107 CMB0=0.182 - 0.019*a_db^(-2.54) + 0.054*a_w^(-0.91);
108
109 % Peak factor
110 g_r=sqrt(2*log(600*f0y)) + 0.5772/(sqrt(2*log(600*f0y)));
111 g_b=g_r;
112
113 % Mode shape correction
114 beta=1.0;
115 phi=(4*alpha+3)/(4*alpha+2*beta+1);
116
117 % Reduced base moment PSD at first mode frequency
118
119 f_p=10^(-5)*(191 - 9.84*a_w + 1.28*a_hr + a_hr*a_w)*(68 - ...
    21*a_db+3*a_db^2);
120
121 s_p=(0.1*a_w^(-0.4) - 0.0004*exp(a_w))*(0.84*a_hr - 2.12 - ...
    0.05*a_hr^2)
122 *(0.422 + a_db^(-1) - 0.08*a_db^(-2));
123

```

```

124 nau=(1 + 0.00473*exp(1.7*a_w))*(0.065+exp(1.26-0.63*a_hr))
125 *exp(1.7-3.44/a_db);
126
127 lambda=(-0.8+0.06*a_w+0.0007*exp(a_w))*(-a_hr^(0.34)+0.00006*exp(a_hr))
128 *(0.414*a_db + 1.67*a_db^(-1.23));
129
130 n0=f0y*w/(mean_speed(end));
131
132 S_M=(s_p*nau*(n0/f_p)^lambda)/((1-(n0/f_p)^2)^2+nau*(n0/f_p)^2);
133
134 % Aerodynamic damping
135
136 damp_a=(0.0025*(1-(1/n0/9.8)^2)*(1/n0/9.8)+0.000125*(1/n0/9.8)^2)/
137 ((1-(1/n0/9.8)^2)^2+0.0291*(1/n0/9.8)^2);
138
139 %Peak factors
140 g_B=zeros(length(x),1);
141 g_R=zeros(length(x),1);
142 p=zeros(length(x),1);
143
144 %Forloop creating the EWSL
145     for j=1:length(x)
146
147         g_B(j)= (0.65 + 1.3*x(j)/H + 7*(x(j)/H)^2 - ...
148                 7.5*(x(j)/H)^3)*g_b*CMB0;
149         g_R(j)=H*m0/Mi *g_r ...
150                 *(x(j)/H)*sqrt((pi()*phi*S_M)/(4*(damping+damp_a)));
151         p(j)=0.5*rho*(mean_speed(j))^2*sqrt(g_B(j)^2 + g_R(j)^2)*w*L ;
152
153     end
154
155 %EWSL on each floor plotted
156 figure()
157 plot(Ptot,x,'-+k',p(:,:),x,'-ok')
158 legend('Along wind','Across-wind')
159 grid on
160
161 end

```

Bibliography

- [1] Kwok K.C.S, Hitchcock P.A, and Butron D.M. Perception of vibration and occupant comfort in wind-excited tall buildings. *Journal of Wind Engineering and Industrial Aerodynamics*, 97:368–380, 2009.
- [2] Hansen R.J, Reed J.W, and Vanmararcke E.H. Human response to wind-incued motion of buildings. *Journal of Structural Division*, ASCE 99(ST7):1589–1605, 1973.
- [3] Denoon R.O, Letchford C.W, Kwok K.C.S, and Morrison D.L. Field measurements of human reaction to wind-induced building motion. In *Proceedings of 10th International Conference on Wind Engineering*.
- [4] Denoon R.O, Roberts R.D, Letchford C.W, and Kwok K.C.S. Field experiments to investigate occupant perception and toleance of wind-induced building motion. *Research Report No R803*, 2000.
- [5] Denoon R.O. *Designing for wind-induced serviceability in buildings*. PhD thesis, The University of Queensland, 2001.
- [6] *Guidelines for the evaluation of of the response of occupants of fixed structures, especually buildings and offshore sturctures, to low-freqyance horizontal motion (0.063 to 1.0 Hz) ISO 6897:1984*.
- [7] Lamb S, Kwok K.C.S, and Walton D. A logitudinal field study of the effects of wind-induced building motion on occupant well-being and work performance. *Journal of Wind Engineering and Industrial Aerodynamics*, 2014.
- [8] Chen P.W and Robertson L.E. Human perception threshold of horizontal motion. *Journal of Structural Divisgion*, 1972.
- [9] Goto T. The criteria to motions in tall buildings (part 1) factors affecting human perception and tolerance of motion. *Transactions of the Architectural Institute of Japan*, 1975.
- [10] A.W Irwin. Perception, comfort and performance criteria for human beings exposed to whole body yaw vibrations and vibrations containing yaw and translational components. *Journal of Sound and Vibrations*, 76(4):481–497, 1981.

- [11] Irwin A.W and Goto T. Human perception, task performance and simulator sickness in single and multi-axis low-frequency horizontal linear and rotational vibration. *United Kingdom informal group meeting on human responses to vibration*, 1984.
- [12] Wong K-S, Hau C.L.V, K.C.S Kwok, and Gonetilleke R.S. Effects of wind-induced tall building vibrations on human motor performance. In *6th European & African Conference on Wind Engineering*.
- [13] Burton M.D, Kwok K.C.S, Hitchcock P.A, and Roberts R.D. Acceptability curves derived from motion simulator investigations and previous experience with building motion. In *Proceedings of 10th Americas Conference on Wind Engineering*.
- [14] Melbourne W.H. and Cheung J.C.K. Designing for serviceable acceleration in tall buildings. In *Proceedings of Fourth International Conference on Tall Buildings*.
- [15] Melbourne W.H and Palmer T.R. Accelerations and comfort criteria for buildings undergoing complex motions. *Journal of Wind Engineering and Industrial Aerodynamics*, 1992.
- [16] Isyomov N. Criteria for acceptable wind-induced motions of tall buildings. In *Proceedings of International Conference on Tall Buildings*.
- [17] National Research Council of Canada, Ottawa, Canada. *National Building Code of Canada. Structural Commentaries (Part 4)*, 1995.
- [18] Burton M.D, Kwok K.C.S, and Abdelrazaq A. Wind-induced motion of tall buildings: Designing for occupant comfort. *International Journal of High-Rise Buildings*, 2015.
- [19] Architectural Institute of Japan, Tokyo, Japan. *Guidelines for the evaluation of habitability to building vibrations, AIJES-V001-2004*, 2004.
- [20] Tamura Y, Kawai H, Uematsu Y, Okada H, and Ohkuma T. Documents for wind resistant design of buildings in Japan. AVECWW.
- [21] *Bases for design of structures - Serviceability of buildings and walkways against vibrations (ISO 10137:2007)*.
- [22] Tony Tschanz. *The Base Balance Measurement Technique And Applications To Dynamic Wind Loading to Structures*. PhD thesis, Western University, 1982.
- [23] John D Holmes. *Wind Loading of Structures*. Taylor and Francis Group, 2015.
- [24] Steenbergen R.D.J.M, Vrouwenvelder A.C.W.M, and Guerts C.P.W. The use of Eurocode EN 1991-1-4 procedures 1 and 2 for building dynamics, a comparative study. *Journal of Wind Engineering and Industrial Aerodynamics*, 2012.
- [25] Alan G Davenport. Gust loading factors. *Journal of the Structural Division*, 93(3):11–34, 1967.

- [26] Kwon D.K and Kareem A. Comparative study of major international wind codes and standards for wind effects on tall buildings. *Engineering Structures*, 2013.
- [27] *Wind Energy Handbook*. John Wileys and Sons, 2001.
- [28] Claës Dyrbye and Svend Ole Hansen. Wind loads on structures. 1996.
- [29] D. Kwon, T. Kijewski-Correa, and A. Kareem. e-analysis of highrise buildings subjected to wind loads. *Journal of Structural Engineering*, 134(7):1139–1153, 2008.
- [30] M Gu and Y Quan. Across-wind loads of typical tall buildings. *Journal of Wind Engineering and Industrial Aerodynamics*, pages 1147–1165, 2004.
- [31] Anil K Chopra. *Dynamics of structures*, volume 3. Prentice Hall New Jersey, 2012.
- [32] The 21st Century Center of Exellent Program. Wind effects on buildings and urban enviroment: Kecture of damping in tall buildings. http://www.wind.arch.t-kougei.ac.jp/info_center/ITcontent/tamura/10.pdf, Cited May 2016.
- [33] Yin Zhou and Ahsan Kareem. Gust loading factor: new model. *Journal of Structural Engineering*, 127(2):168–175, 2001.
- [34] A. Lago, D. Trabucco, and A. Wood. Damping technologies for tall buildings: New trends in comfort and safety. <https://www.elsevier.com/physical-sciences/engineering-and-technology/damping-technologies-for-tall-buildings-new-trends-in-comfort-and-safety>, Cited May 2016.
- [35] B. Samali and K.C.S Kwok. Use of viscoelastic dampers in reducing wind- and earthquake-induced motion of building structures. *Engineering Structures*, 1995.
- [36] David Lee and Douglas P Taylor. Viscous damper development and future trends. *The Structural Design of Tall Buildings*, 10(5):311–320, 2001.
- [37] Yongqi Chen, Cheng Peng, Hengli Xue, and Liangzhe Ma. The function and economic effective of fluid viscous dampers to reduce seismic and wind vibrations in high-rise buildings.
- [38] Jermony Connor. *Introduction to Structural Motion Control*. Prentice Hall, 2002.
- [39] Ahsan Kareem. Reduction of wind induced motion utilizing a tuned sloshing damper. *Journal of Wind Engineering and Industrial Aerodynamics*, 36:725–737, 1990.
- [40] MJ Hochrainer. Tuned liquid column damper for structural control. *Acta Mechanica*, 175(1-4):57–76, 2005.

- [41] H Cao and QS Li. New control strategies for active tuned mass damper systems. *Computers & structures*, 82(27):2341–2350, 2004.
- [42] H Cao, AM Reinhorn, and TT Soong. Design of an active mass damper for a tall tv tower in nanjing, china. *Engineering Structures*, 20(3):134–143, 1998.
- [43] JN Yang, JC Wu, and Z Li. Control of seismic-excited buildings using active variable stiffness systems. *Engineering Structures*, 18(8):589–596, 1996.
- [44] Tadashi Nasu, Takuji Kobori, Motoichi Takahashi, Naoki Niwa, and Katsura Ogasawara. Active variable stiffness system with non-resonant control. *Earthquake engineering & structural dynamics*, 30(11):1597–1614, 2001.